CHALMERS

Modelling For Competitor Vehicle Analysis

Master's thesis in Applied Mechanics

MARTIN LJUNGGREN
GUNNAR SAHLIN

Department of Applied Mechanics
Division of Vehicle Engineering and Autonomous Systems
Group of Vehicle Dynamics
CHALMERS UNIVERSITY OF TECHNOLOGY
Göteborg, Sweden 2016

MASTER'S THESIS IN APPLIED MECHANICS

Modelling For Competitor Vehicle Analysis

MARTIN LJUNGGREN
GUNNAR SAHLIN

Department of Applied Mechanics
Division of Vehicle Engineering and Autonomous Systems
Group of Vehicle Dynamics
CHALMERS UNIVERSITY OF TECHNOLOGY

Göteborg, Sweden 2016

Modelling For Competitor Vehicle Analysis
MARTIN LJUNGGREN
GUNNAR SAHLIN

Master's thesis 2016:29
ISSN 1652-8557
Department of Applied Mechanics
Division of Vehicle Engineering and Autonomous Systems
Group of Vehicle Dynamics
Chalmers University of Technology
SE-412 96 Göteborg
Sweden
Telephone: +46 (0)31-772 1000

Cover:
Steering Robot Test, url: spectrum.ieee.org/image/520218
Volvo Cars Driving Simulator, url: *www.media.volvocars.com/image/low*/167930/1_1/5?$i = 1$

Chalmers Reproservice
Göteborg, Sweden 2016

Modelling For Competitor Vehicle Analysis
Master's thesis in Applied Mechanics
MARTIN LJUNGGREN
GUNNAR SAHLIN
Department of Applied Mechanics
Division of Vehicle Engineering and Autonomous Systems
Group of Vehicle Dynamics
Chalmers University of Technology

Abstract

This thesis describes the development and evaluation of a competitor vehicle model for Volvo Cars Corporation's moving base driving simulator. Vehicle simulations are important when aiming for decreased development time within the vehicle industry. Simulations help the engineers to front-load projects, thereby improving efficiency and product quality. To remain competitive it is essential to know the industry's state of the art technology. One commonly used method is competitor analysis. The thesis delivers a method of how to measure a competitor's vehicle in order to create a vehicle model that can be tested objectively in VI-CarRealTime as well as subjectively in a driving simulator. This gives the opportunity to save the competitor vehicle in a database and perform tests even if the physical vehicle is no longer available. The thesis focuses mainly on capturing the lateral tyre and steering characteristics of the competitor vehicle with the main priority to mimic the full vehicle behaviour while minimising additional requirements needed compared to a standard measuring. It is favourable to separate the different system in the full vehicle model in order to facilitate the vehicle analysis on component level. Two methods are presented and carried out. One named Measurement Based Method that requires measured tie-rod forces using strain gauge sensors on the tie-rods as an additional measuring equipment. The second method named Estimation Based Method is using the standard measuring equipment but instead requires a Brush Tyre Model to correlate lateral tyre characteristics to aligning torque. The advantage of knowing the tie-rod forces is that tyres and the steering system can be completely decoupled from each other which gives higher accuracy on component level. The tyre model is optimised so that the simulated vehicle shows the same response as the measured vehicle in a series of manoeuvres. The lateral tyre parameters are assumed to be found when the vehicle model is achieving the same yaw rate and lateral acceleration as for the physical vehicle in an identical manoeuvre. A steering algorithm is designed to imitate the behaviour of vehicle's power steering system by estimating the relation between rack force and steering wheel torque. The resulting steering algorithm is tuned to simulate the wanted steering system by adjusting damping and friction parameters together with a base torque given by a velocity versus rack force dependent look-up table. Objective evaluations show good correlation for low transient manoeuvres. However, at higher transients the tuned models differentiated more from the measured data. The Measured Based Method was thought to have higher accuracy when evaluating subjectively which resulted in it to become the favourable method. Further work needs to be carried out on both the steering system and the tyre optimisation in order to have an established method.

Keywords: Vehicle model, Competitor vehicle, VI-CarRealTime, Volvo Cars, Driving simulator, Vehicle dynamics, XC90, Tyre parametrisation, Torque feedback

Acknowledgements

Thanks to Volvo Cars Corporation, department of Vehicle Dynamics CAE. Supervisors Carl Sandberg, Anton Albinsson and examiner Mathias R Lidberg. Sergej Abyzov and the measuring crew for the measurements performed at Hällered proving ground. We would also like to show gratitude to Max Boerboom and Marcus Ljungberg for good guidance in tyre and steering modelling and for their contribution in the subjective test sessions.

Abbreviations

Volvo Cars Volvo Car Corporation

CRT VI-CarRealTime

OEM Original Equipment Manufacturer

SWA Steering Wheel Angle

SWV Steering Wheel Velocity

SWT Steering Wheel Torque

OC On Centre

HSS High g Swept Steer

CR Constant Radius

SPMM Suspension Parameter Measurement Machine

K&C Kinematic and Compliance

NVH Noise Vibration Harshness

ADAS Advanced Driver Assistance Systems

EPS/EPAS Electric power steering/ Electric Power Assisted Steering

HPAS Hydraulic Power Assisted Steering

EHPAS Electric Hydraulic Power Assisted Steering

List of Figures

List of Tables

Contents

1 Introduction

This thesis describes the development and evaluation of a competitor vehicle model for Volvo Cars' moving base driving simulator. The current method used when benchmarking competitor's vehicles contains both subjective testing performed by professional drivers as well as objective testings performed in rigs and by a steering robot. Competitor's vehicles are only available for a limited time which results in that a limited amount of tests can be performed. Standard tests with the steering robot consists of a number of manoeuvres performed in order to get a foundation for vehicle evaluation and comparison. This thesis aims to deliver a method of what measurements that are needed in order to create a competitor's vehicle model. The use of a vehicle model of a competitor vehicle will allow subjective evaluation in the driving simulator at Volvo Cars. Driving in the simulator is not the same as driving in reality, but the driver gets an indication of the vehicle feel and comparison between different models is possible. A competitor vehicle model will also enable objective evaluations to be performed. Volvo Cars is then no longer limited to the manoeuvres performed when the vehicle was available.

The thesis focuses on capturing the steering torque and lateral tyre characteristics in order to imitate the handling and steering characteristics of the competitor vehicle. Challenges when modelling a competitor's vehicle compared with a Volvo Cars vehicle is primary due to the lack of design data, software and limited availability. Tyre data is often received by using external tyre measuring services. Savings within cost and time can be made by having a method to tune tyres in order to achieve the same vehicle behaviour in simulations as well as for manoeuvres performed on a test track. Information about the power steering system for a Volvo Cars vehicle is imported from existing models in Adams, [2]. This is not achievable when modelling a competitor vehicle. A method of how to simulate steering wheel torque in relation to vehicle velocity and steering rack force as well as steering wheel velocity is therefore developed and evaluated in this thesis.

1.1 Background

The vehicle industry is working towards evaluating and testing vehicle dynamics earlier in the developing process using computer aided engineering tools such as simulation software and driving simulators. This allows optimisations to be done in an earlier state of the development process which reduces both cost and development time. Benchmarking of other vehicle brands is a common way to keep up with the technology trends and to earn knowledge. Using driving simulators for evaluation of vehicle characteristics requires a representative vehicle model. Volvo Cars measures many of the parameters needed for vehicle modelling in the current method. Parameters for kinematics and compliance, mass and inertia as well as damper characteristics are measured on different rigs. full-vehicle ride and handling characteristics are measured on test tracks. Two important sub-systems that are not explicitly identified in the current benchmarking process are the power steering and tyre characteristics. Volvo Cars is therefore interested in a method to characterise these using mainly existing test methods.

The common way to perform full vehicle benchmarking is to evaluate the vehicle both subjectively and objectively. Subjective evaluation usually consists of scoring different aspects of the vehicle characteristics. For objective evaluation it is common to gather data from standardised test performed on test tracks. Acar and Ulaş shows in their paper how full vehicle benchmarking can be performed and how the data can be used as a reference in vehicle development [1]. Kinstle et al. shows how one can use data received from benchmarking to parametrise a vehicle model and perform sensitivity analysis in a vehicle stability point of view [8].

1.2 Deliverables

- Evaluate if existing methods and techniques can be combined to improve model correlation and driving characteristics in a driving simulator.
- Description of the parametrisation of a competitor vehicle
- Implement the parametrisation of a competitor vehicle in a VI-CarRealTime model.
- Perform validation testing by offline simulation and driving in the driving simulator.

1.3 Scope

The main purpose of this thesis was to develop a method of how to parametrise the driving characteristics of a competitor vehicle and be able to drive it in a driving simulator at Volvo Cars. This was carried out by performing physical measurements and building a simulation model in the vehicle simulation tool VI-CarRealTime with additional steering system modelling in Matlab/simulink. The developed method focuses on capturing the full vehicle behaviour although a deeper knowledge about sub-systems also favours the competitor vehicle analysis. Steering feedback torque and lateral tyre characteristics was the sub attributes with the highest focus in this thesis.

1.4 Delimitation

The developed method will handle vehicles with all four wheels of the same type, with a constant steering ratio between rack and steering wheel except for the non-linearity created from the universal joints in the steering column. Measuring a competitor vehicle will not require any changes to the vehicle that are not resettable nor will they require more than two extra days of testing compared to a standard DNA-measurement. Tyre estimation will only be performed in the lateral direction and the parameters depending on the camber angle will not be optimised.

2 Theory

This chapter contains the theory about different systems treated in this thesis. It introduces fundamental equations and relations within vehicle dynamics. Different steering assist systems as well as suspension parameters will be explained on a basic level. Theory about tyre characteristics will be presented in this chapter as well as tyre modelling for both semi-empirical and physical tyre models. The software and the rigs that were used during the thesis will be introduced. Brief information about the optimisation tools used will be shown at the end of the chapter.

2.1 Suspension setup

Suspensions can be modified in many ways to reach the wanted dynamic properties of the vehicle. In this report the suspension characteristics described follows the definition of the SPMM-rig calculation manual, [3], due to the measurement data acquired follows these definitions. The parameters describing the alignment of the suspension is Toe angle, Caster angle, King-pin angle and Camber angle will be explained separately in the following sections.

2.1.1 King-pin angle and King-pin offset

King-pin axis is the axis which the wheel rotates around when turning, seen in figure 2.1. In a double wishbone suspension the King-pin axis is defined as the axis between the joint in the upper and lower wishbone. In a MacPherson front suspension the King-pin axis is defined as the axis between the upper mount of the strut and the lower outer ball joint. The King-pin offset is here defined as the distance between the contact point between centre of wheel and ground to the contact point between the King-pin axis and ground. The King-pin offset is depicted in the top view in figure 2.3.

2.1.2 Caster angle and Mechanical trail

The Caster angle is the inclination of the King-pin axis in the vertical plane seen from the side as in figure 2.2. In figure 2.2 and 2.3 the Mechanical trail, sometimes called the Caster offset is depicted. It is defined as the distance between the King-pin axis ground contact and the contact between centre of the wheel ground contact, [13]. The Mechanical trail acts as an lever arm of the lateral tyre force which affects the steering characteristics. The Mechanical trail increases with an increasing Caster angle. The length of the Mechanical trail tends to affect the stability of the vehicle, a larger Mechanical trail results in a more stable vehicle but increases the steering effort. A shorter Mechanical trail requires less steering effort but with the drawback of less stability.

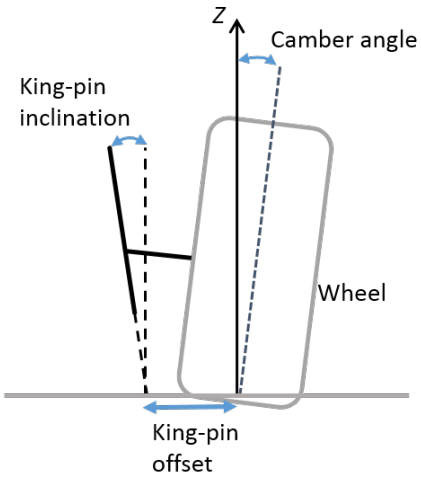

Figure 2.1: King-pin inclination and King-pin offset seen the tyre in front view

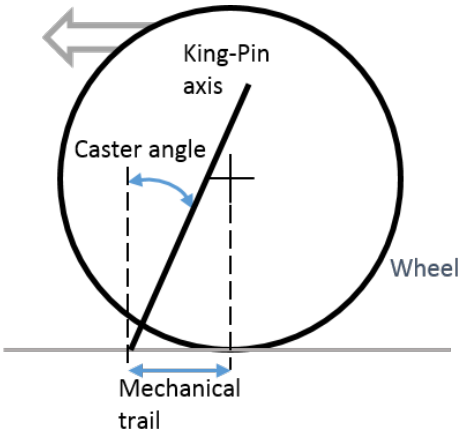

Figure 2.2: King-pin axle and Caster angle with defined Mechanical trail. Seen the tyre from side view

2.1.3 Camber angle

Camber angle is the inclination of the tyre refereed to the vertical axis as in figure 2.1. The camber angle is here defined as negative if the wheel leans in towards the chassis and positive if it leans outwards. The Camber angle influences the lateral tyre characteristics and is normally set to be around 0.5-1 degrees negative for normal road vehicles [15]. In this thesis the effect of Camber is not considered.

2.1.4 Toe angle

The Toe angle is depicted in figure 2.4. It is defined as the angle the wheels have with a straight steering wheel seen from above. Toe-in is defined as both wheels on an axle are pointing inwards and is also called positive Toe angle. Toe-out is the opposite with the wheels pointing outwards resulting in negative Toe angles. On a passenger vehicle the Toe angle is often positive on both the front and rear axle, [7]. Toe-in on the front axle tends to give higher yaw stability while toe-out increases the yaw response. The rear axle has commonly toe-in to counteract over steer. Large Toe angles increases the rolling resistance and the wear of the tyre, [7].

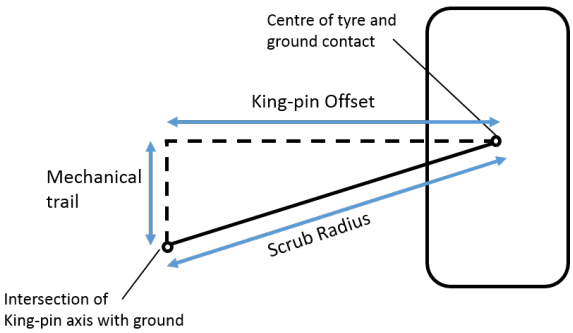

Figure 2.3: Tyre in top view showing Scrub radius, King-pin offset and Mechanical trail

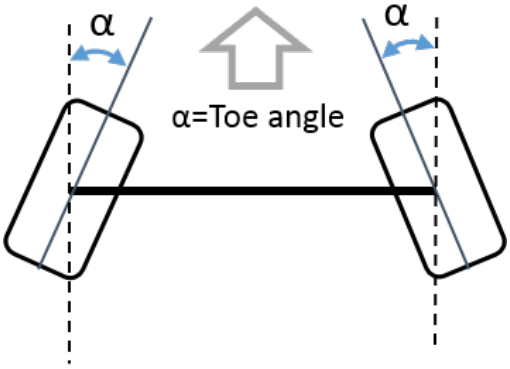

Figure 2.4: Top view of the front axle with clarified Toe angles

2.2 Tyre characteristics

There are multiple methods how to derive the tyre characteristics of a tyre. The most common methods are either to derive a physical model that describes the characteristics of the tyre or to derive a semi-empiric model through curve-fitting tyre data received from a tyre test rig [10]. Important terms when studying lateral characteristics are lateral force, pneumatic trail, aligning torque and relaxation length. The important terms will be explained more in the following sections. Figure 2.5 shows an overview over how the lateral force, F_y, and the aligning torque, M_z, can be seen as a function of side slip angle ,α. The cornering stiffness, $C_{F\alpha}$, can be seen as the inclination of the linear region of the lateral force. To the right is the coordinate system for the tyre displayed with the longitudinal force, F_x, normal load, F_z, rotational velocity, Ω and velocity V denoted.

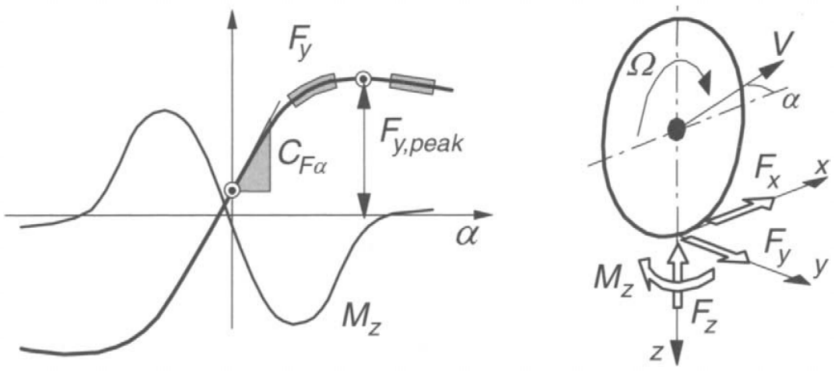

Figure 2.5: Overview of tyre coordinate system as well as force and torque curves, [10]

2.2.1 Lateral Force

Lateral force is induced in the tyre contact patch when a side slip angle is created on the tyre. The lateral force can be seen as having a linear region at low side slip angle and of which the inclination is called cornering stiffness, $C_{F\alpha}$. The cornering stiffness can be seen in figure 2.5 [10]. The lateral force enters at a higher side slip angle a non-linear region where the inclination is reduced as the side slip angle increases. This results in that the lateral force reaches a peak value and with further increased side slip angle the lateral force often starts to reduce.

2.2.2 Pneumatic Trail

The centre of the resultant lateral force does most often occur behind of the wheel centre. The distance between these is called pneumatic trail. This pneumatic trail times the resultant lateral tyre force means an essential part of the aligning torque around the wheel centre. The pneumatic trail distance has its highest value when the side slip angle is zero, if no shift effects is considered, and decays as the side slip angle increases, [10].

2.2.3 Aligning Torque

The aligning torque is defined as the lateral force times the pneumatic trail. In the front suspension this torque is taken up by the tie-rod force. This force is translated into the steering rack and transformed into steering wheel torque. The aligning torque is therefore one of the main sources of steering feedback to the driver.

2.2.4 Relaxation Length

Relaxation length is a measurement that determines how long it takes for the tyre to achieve steady state forces when induced by a slip angle [9]. both longitudinal and lateral relaxation behaviour exists. This section will introduce an approximation of the relaxation length following the paper of J.S. Loeb et al. [9]. Figure 2.6 shows a wheel that is steered around a point P with a steering angle of δ.

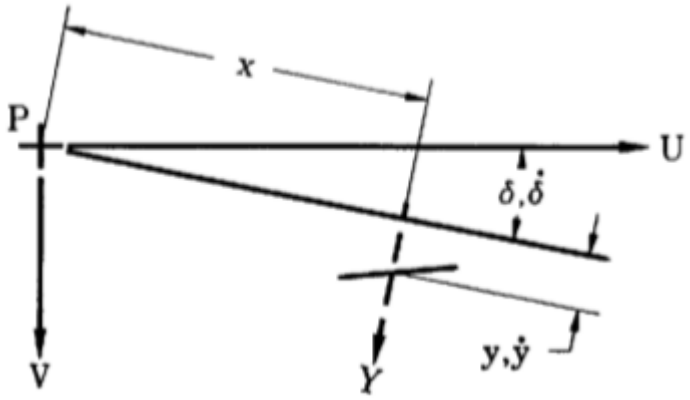

Figure 2.6: Forces and angles seen in top view of a tyre on top of a moving ground used for determining the relaxation length, [9]

where U and V are the longitudinal and lateral velocity respectively at the tyre rotation point, P. $\delta, \dot{\delta}$ are the steer angle and steer velocity between the longitudinal velocity of the moving ground and the longitudinal velocity of the tyre. The deflection and the rate of deflection of the tyre are noted y and $\dot{y}$. Most of the tyre deflection comes from tyre carcass deflection but some also comes from thread deflection. x is the trail from point P to where the lateral force, Y, is acting. The rate of steer angle and rate of deflection are defined as equation 2.1.

$$\dot{\delta} = \frac{d\delta}{dt} \qquad \dot{y} = \frac{dy}{dt} \tag{2.1}$$

The cornering stiffness and lateral stiffness is defined as equation 2.2.

$$C_{F\alpha} = \frac{dF_y}{d\delta} \qquad C_{Fy} = \frac{dF_y}{dy} \tag{2.2}$$

The lateral force can be expressed both as equation 2.3 states as a product of cornering stiffness and slip angle or as equation 2.4 shows as a product of lateral stiffness and tyre deflection. Note that small steer angles are assumed.

$$F_y = C_{F\alpha} \cdot \left(\delta - \frac{(V + x \cdot \dot{\delta} + \dot{y})}{U} \right) \tag{2.3}$$

$$F_y = C_{Fy} \cdot y \tag{2.4}$$

Equation 2.3 and 2.4 combined will result in equation 2.5.

$$C_{Fy} \cdot y = C_{F\alpha} \cdot \left(\delta - \frac{(V + x \cdot \dot{\delta} + \dot{y})}{U} \right) \tag{2.5}$$

The first-order differential equation can be rewritten as equation 2.6 shows:

$$\dot{y} \cdot \frac{U \cdot C_{Fy}}{C_{F\alpha}} \cdot y = U \cdot \delta - V - x \cdot \dot{\delta} \tag{2.6}$$

A step steer can be used as the steer input of equation 2.6 which results in following steering function, equation 2.7.

$$\delta = S \qquad for\ t > 0 \tag{2.7}$$

Equation 2.6 will be simplified by assuming zero side slip velocity, V, and zero trail, x, which gives equation 2.8.

$$\dot{y} = -\frac{U \cdot C_{Fy}}{C_{F\alpha}} \cdot y + U \cdot S \qquad for\ t > 0 \tag{2.8}$$

The solution for the differential equation of equation 2.8 can be seen in equation 2.9.

$$y = \frac{S \cdot C_{F\alpha}}{C_{Fy}} \cdot \left(1 - \exp\left(\left(\frac{-U \cdot C_{Fy}}{C_{F\alpha}}\right) \cdot t\right)\right) \tag{2.9}$$

And the lateral force can be written as equation 2.10.

$$F_y = S \cdot C_{F\alpha} \cdot \left(1 - \exp\left(\left(\frac{-U \cdot C_{Fy}}{C_{F\alpha}}\right) \cdot t\right)\right) \tag{2.10}$$

The rise time for the exponential equation is, $\tau = C_{F\alpha}/(U \cdot C_{Fy})$, which results in that the relaxation length, σ_α which is the rise time multiplied with the velocity can be written as equation 2.11.

$$\sigma_\alpha = \frac{C_{F\alpha}}{C_{Fy}} \tag{2.11}$$

2.2.5 Brush Model

The Brush Model is a simple physical tyre model where no compliance is considered and the tyre carcass is assumed rigid. These simplifications influence the result noticeable and results in a less accurate model compared to other tyre models. The advantages for the Brush model is that the number of unknowns is reduced significant compared to more advanced models.

According to the brush model the tyres consists of elastic bristles, also called treads, that deforms when entering the contact patch resulting in that a reaction force occurs between the road and the tyre [10]. It is assumed that the treads enters the contact patch perpendicular to the road surface and will adhere to the ground as long as sufficient friction exists. Figure 2.7 shows the the brush model from a top and side view at pure side slip condition.

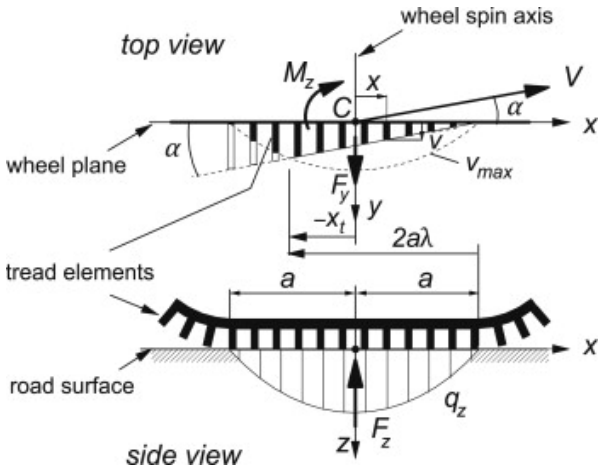

Figure 2.7: Brush Model for pure side slip from a top and side view [10]

The Brush Model assumes a parabolic pressure distribution of q_z in the contact patch according to equation 2.12 which can also be seen in figure 2.7 [10].

$$q_z = \frac{3 \cdot F_y}{4 \cdot a} \cdot \left(1 - \left(\frac{x}{a}\right)^2\right) \tag{2.12}$$

Where F_z is the normal load, a is half the contact patch length and x is the distance from the wheel spin axis to the point in the contact patch which is studied. The maximum lateral force distribution is calculated by multiplying the normal load distribution with the friction, equation 2.13.

$$|q_{y,max}| = \mu \cdot q_z = \frac{3}{4} \cdot \mu \cdot F_z \cdot \frac{(a^2 - x^2)}{a^3} \tag{2.13}$$

Consequently the maximum deflection v_{max} over the contact patch will have the same parabolic shape as the normal load and the lateral force distribution which results in equation 2.14 [10].

$$v_{max} = \frac{\mu \cdot q_z}{c_{py}} = \frac{q_{y,max}}{c_{py}} \tag{2.14}$$

The treads will increase its deformation as it moves further into the contact patch resulting in that the maximum deflection first will occur at the trailing edge. This results in that two regions is created in the contact patch, one region where the threads still adheres to the ground and one region where the threads have reached the maximum deformation and is now sliding. As the longitudinal or lateral slip increases the area that reaches maximum deflection will grow toward the leading edge[10]. The deformation at the adhesion regions of the contact patch that has not achieved full deformation is assumed to follow a tangent function which can be seen in equation 2.15 and can be seen in figure 2.7.

$$v = (a - x) \cdot \tan(\alpha) \tag{2.15}$$

The lateral force is dependant of the side slip angle where increased side slip angle generates a larger lateral force. As the side slip angle increases a larger part of the contact patch will saturate, meaning it will reach its maximum deflection. In the areas where maximum deflection is achieved the treads will start to slide instead of adhere to the ground. When the whole contact patch is sliding the wheel has utilised maximum friction and further increase of slip angle would not result in higher lateral force [10]. Figure 2.8 shows how the contact patch is utilised for different side slip angles and how the resultant F_y moves toward the centre of the contact patch as the side slip angle increases.

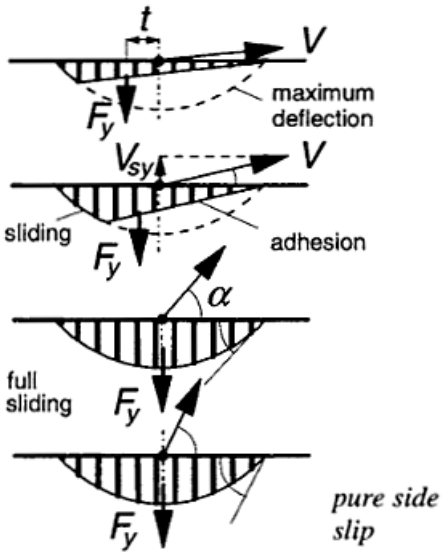

Figure 2.8: Utilized contact patch for different side slip angles for a Brush Model

The lateral force is defined as shown in equation 2.16 [10]:

$$F_y = c_{py} \int_{-a}^{a} v \, dx = 2 \cdot c_{py} \cdot a^2 \cdot \alpha \tag{2.16}$$

where c_{py} is lateral stiffness per unit length, v is the deflection and a is half the contact patch length. For the aligning torque the equation becomes accordingly to equation 2.17:

$$M_z = c_{py} \int_{-a}^{a} v \cdot x \, dx = -\frac{2}{3} \cdot c_{py} \cdot a^3 \cdot \alpha \tag{2.17}$$

The Cornering stiffness and aligning stiffness becomes accordingly to equation 2.18 and equation 2.19 respectively:

$$C_{F\alpha} = \left(\frac{\partial F_y}{\partial \alpha} \right)_{\alpha=0} = 2 \cdot c_{py} \cdot a^2 \tag{2.18}$$

$$C_{M\alpha} = -\left(\frac{\partial M_z}{\partial \alpha} \right)_{\alpha=0} = \frac{2}{3} \cdot c_{py} \cdot a^3 \tag{2.19}$$

It is common to introduce the parameter Θ_y, equation 2.20, resulting in that equation 2.13 becomes 2.21.

$$\Theta_y = \frac{2 \cdot c_{py} \cdot a^2}{3 \cdot \mu \cdot F_z} \tag{2.20}$$

$$|q_{y,max}| = \frac{c_{py}}{2 \cdot a \cdot \Theta_y} \cdot (a - x) \cdot (a + x) \tag{2.21}$$

A factor λ is introduced that determines the ratio between the adhesion region and the sliding region of the contact patch. λ is defined as equation 2.22 shows, where x_t is the distance from the wheel spin axis to the where the sliding region begins.

$$\lambda = \frac{a - x_t}{2 \cdot a} \tag{2.22}$$

The λ factor multiplied with the contact patch length, $2a\lambda$, defines the point of where the adhesion region stops and the sliding region starts. This result in that a λ-value of 0 represents fully sliding while a λ-value of 1 means fully adhesion at the contact patch. At the point of where the sliding region starts, $x = x_t$ the lateral force distribution will be the same when calculating it as an adhesion lateral force as well as a sliding lateral force. This results in that the equation 2.23 must be valid.

$$\begin{aligned}
|q_y| = c_{py} \cdot (a - x_t) \cdot |\tan(\alpha)| = |q_{y,max}| &= \frac{c_{py}}{2 \cdot a \cdot \Theta_y} \cdot (a - x_t) \cdot (a + x_t) \\
c_{py} \cdot (a - x_t) \cdot |\tan(\alpha)| &= \frac{c_{py}}{2 \cdot a \cdot \Theta_y} \cdot (a - x_t) \cdot (a + x_t) \\
|\tan(\alpha)| &= \frac{1}{2 \cdot a \cdot \Theta_y} \cdot (a + x_t) \\
\Theta_y \cdot |\tan(\alpha)| - 1 &= \frac{(a + x_t)}{2 \cdot a} - 1 \\
1 - \Theta_y \cdot |\tan(\alpha)| &= \lambda
\end{aligned} \tag{2.23}$$

From the expression received by equation 2.23 one can determine at which side slip angle complete sliding is achieved by setting $\lambda = 1$, equation 2.24.

$$\tan(\alpha_{sl}) = \frac{1}{\Theta_y} \tag{2.24}$$

With a defined deflection distribution both for the adhesion region and the sliding region as well as where the transition occurs the lateral force and aligning torque can be integrated over the contact patch [10]. $\sigma_y = tan(\alpha)$ is often introduced for simplicity when writing out equation 2.25 and 2.26.

$$F_y(\alpha) = \begin{cases} \mu F_z (1 - \lambda^3) \cdot \text{sign}(\alpha) = 3\mu F_z \Theta_y \sigma_y \left(1 - |\Theta_y \sigma_y| + \frac{1}{3}(\Theta_y \sigma_y)^2\right) & \textit{When } |\alpha| \leq \alpha_{sl} \\ \mu F_z \cdot sign(\alpha) & \textit{When } |\alpha| > \alpha_{sl} \end{cases} \tag{2.25}$$

$$M_z(\alpha) = \begin{cases} -\mu F_z \lambda^3 a (1 - \lambda) \cdot \text{sign}(\alpha) = -\mu F_z a \Theta_y \sigma_y \left(1 - 3|\Theta_y \sigma_y| + 3(\Theta_y \sigma_y)^2 - |\Theta_y \sigma_y|^3\right) & \textit{When } |\alpha| \leq \alpha_{sl} \\ 0 & \textit{When } |\alpha| > \alpha_{sl} \end{cases} \tag{2.26}$$

With the lateral force and the aligning torque now defined the pneumatic trail can be expressed as in equation 2.27.

$$t(\alpha) = \frac{M_z(\alpha)}{F_y(\alpha)} = \begin{cases} \frac{1}{3} a \frac{1 - 3|\Theta_y \sigma_y| + 3(\Theta_y \sigma_y)^2 - |\Theta_y \sigma_y|^3}{1 - |\Theta_y \sigma_y| + \frac{1}{3}(\Theta_y \sigma_y)^2} & \textit{When } |\alpha| \leq \alpha_{sl} \\ 0 & \textit{When } |\alpha| > \alpha_{sl} \end{cases} \tag{2.27}$$

2.2.6 Magic Tyre Formula Model

The Magic Tyre Formula is a semi-empirical method designed to capture the characteristics of a tyre. The formula was derived to be used to curve-fit tyre data and by that be able to use an

equation determining the tyre characteristic. The formula is used to derive different properties such as lateral force, longitudinal force and aligning torque. The complexity and number of coefficients in the equation rises depending on the detail of curve-fit. When all coefficients are determined from tyre testing the equation can be used to calculate the wanted properties.

The curve produced from the Magic Tyre Formula rarely passes through the origin of the coordinate system. This is due to asymmetry within the tyre and results in an offset from the origin, called shifts. The variables S_V and S_H are introduced to capture these properties. The general form of the Magic Tyre Formula equation is seen in 2.28.

$$y = D \cdot \sin[C \cdot \text{atan}\{Bx - E(Bx - \text{atan}(Bx)\}] \tag{2.28}$$

with:

$$Y(x) = y(x) + S_V \tag{2.29}$$

$$x = X + S_H \tag{2.30}$$

The general form applies for the following definition of the parameters, [10].

Y: Output variable. Ex: $F_x or F_y$

X: Input variable. Ex: slip ratio or side slip

B: Stiffness factor

C: Shape factor

D: Peak value

E: Curvature factor

S_H Horizontal shift

S_V Vertical shift

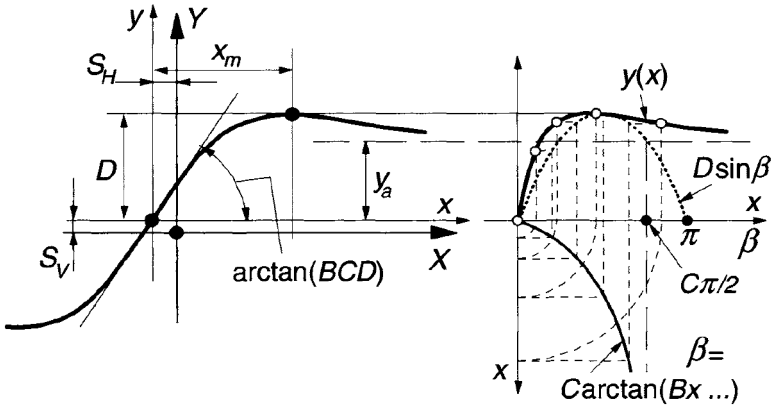

Figure 2.9: Overview of sine version for Magic Tyre Formula, [10]

The product from multiplying the constants B, C and D will result in the cornering stiffness of the tyre.

The aligning torque can be derived by multiplying the pneumatic trail, equation 2.31, with the lateral force and adding the residual torque, equation 2.34, as equation 2.32 states. When calculating

the pneumatic trail the cosine version of the Magic Tyre Formula is used. The pneumatic trail has its peak at $\tan\alpha = -S_{Ht}$ [10]. The residual torque is a function of α_r, equation 2.35, which is the side slip angle multiplied with a shift factor. Note that the factors B,C,D, and E differs between aligning torque, longitudinal force and lateral force equation of the Magic Tyre formula.

$$t(\alpha_t) = D_t \cdot \cos[C_t \cdot \text{atan}\{B_t \cdot \alpha_t - E_t(B_t \cdot \alpha_t - \text{atan}(B_t \cdot \alpha_t)\}] \tag{2.31}$$

$$M_Z = -t \cdot F_y + M_{ZR} \tag{2.32}$$

$$\alpha_t = \tan(\alpha) + S_{Ht} \tag{2.33}$$

$$M_{ZR}(\alpha_r) = D_R \cdot \cos[\text{atan}(B_r \alpha_r)] \tag{2.34}$$

$$\alpha_r = \tan(\alpha) + S_{Hf} \tag{2.35}$$

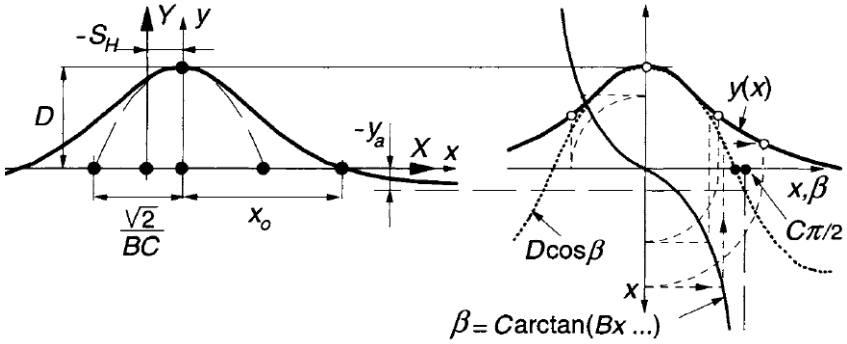

Figure 2.10: Overview of cosine version of Magic Tyre Formula , [10]

The extended Magic Tyre Formula equations for lateral force and aligning torque can be seen in appendix A.

2.3 Steering System Design

The steering system treated in this thesis consists of a rack and pinion configuration and is a common steering system on passenger cars as well as on heavier vehicles [11]. The steering system consists of a pinion mounted on the steering column and a rack that is connected through tie-rods to the wheel uprights with an offset to the turning axis. The tie-rods are mounted with ball joints to the rack and to the wheel upright. Rotational motion of the steering column is transformed via the pinion gear into translation motion on the rack. Due to the offset of the tie-rod mounting to the wheel upright the translation motion on the rack creates a rotational motion on the wheel [11]. Advantages with this steering system are that it is a simple design and is both compact and causes minimal steering compliance [11].

Most vehicles of today are equipped with a power assist system which is mounted on the rack or the steering column and assists the driver during turning manoeuvres. The power assist system applies additional torque to rack to help the driver manoeuvre easier and can be noticed clearly when driving at low speeds for instance during parking manoeuvres. Figure 2.11 shows an overview of a rack and pinion steering system with power assist.

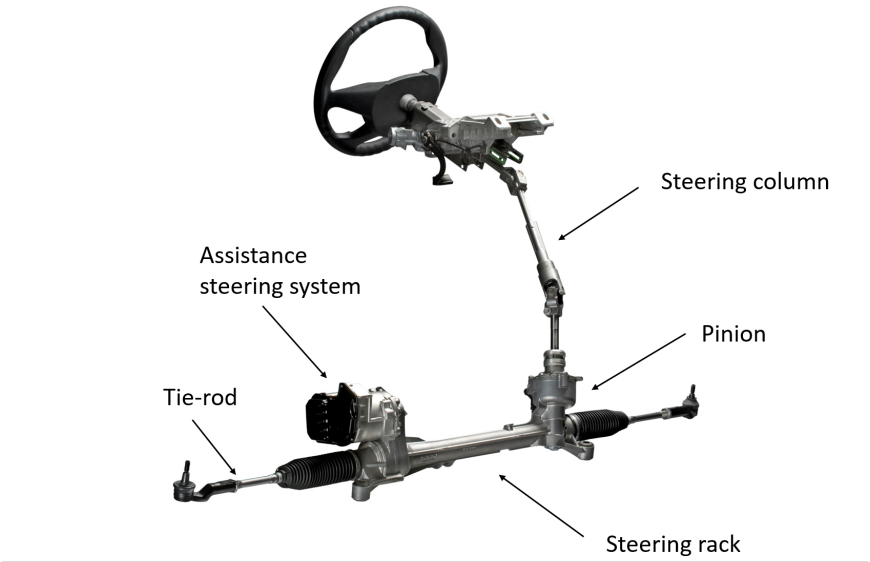

Figure 2.11: Overview of a steering rack and pinion configuration, [5]

Car manufacturers aim to reduce the steering compliance in the steering column which results in a more responsive system. Therefore a torsional stiff steering column is beneficial which will reduce the flexibility [11].

Due to packaging and ergonomics a straight column is not achievable and universal joints are typically used to allow angular deflection. These joints introduce a non linear dependency between the steering wheel angle and rack displacement. This is due to the input shaft and the output shaft of the steering column is not parallel to each other which results in that there will not be a constant rotation on the steering pinion. Depending on how one design the system the steering ratio can either increase or decrease on increased steering wheel angle. The output rotational velocity, ω_{out}, can be seen in equation 2.36.

$$\omega_{out} = \frac{\omega_{in} \cdot \cos(\Theta)}{1 - \sin^2(\alpha) \cdot \sin^2(\Theta)} \tag{2.36}$$

where ω_{in} is the rotational velocity into the universal joint and Θ is the angle between the input shaft and the output shaft and α is where around the output shaft the rotational velocity is studied [4].

2.3.1 Hydraulic Power Assisted Steering

Hydraulic Power Assisted Steering, HPAS, uses a hydraulic pump that is driven by the engine shaft. The hydraulic pump creates a equal pressure on both sides of a piston that is mounted on the steering rack. A valve is mounted on the steering pinion which opens when the steering wheel is turned. When the valve opens the hydraulic system increase the flow into one side of the piston resulting in a pressure difference. This pressure difference creates an additional force on the steering rack helping the driver to turn [16]. An advantage of the HPAS is that it can create large assistance force while disadvantages is that the hydraulic pump uses energy from the engine shaft which needs to constantly be running to contain the pressure on the both sides of the piston. The hydraulic system requires a large space which is also a disadvantages, [16]. Active steering systems such as lane keeping aid, park assist and future autonomous driving is not possible with this system.

2.3.2 Electric Hydraulic Power Assisted Steering

Electric Hydraulic Power Assisted Steering, EHPAS, uses a electric motor to operate the hydraulic pump and therefore does not need to be connected to the drive shaft. The advantage over HPAS is that the electric motor can run on low rpm or even shut off when driving straight ahead saving energy [16]. When turning the electric motor increases its rpm and gives sufficient steering assist. EHPAS shares the incompatibility of HPAS towards active assistance systems.

2.3.3 Electric power steering

Electric Power Steering, EPS, also called Electric Power Assisted Steering, EPAS, is becoming more popular and opens up for a lot of opportunities. The electric motor that is used to provide assist torque is either connected to the rack or the steering column, [12]. The electric power steering is more energy efficient than convectional systems. EPS/EPAS enables interventions from active systems like lane keeping assist, autonomous drive and parking aid. The electric system is also programmed to give different torque depending on situations, often according to vehicle velocity, steering wheel torque as well as steering wheel angle. The relation between assist torque applied versus driver's steering wheel torque called boost curves are tuned to give the driver a positive torque feedback.

2.4 Moving Base Driving Simulator

Volvo Cars is using a moving base simulator from VI-grade s.r.l. including a motion platform manufactured by SAGINOMIYA SEISAKUSHO, INC. The simulator is of the type called Driver-in-Motion, *DiM*. It consist of a base platform that moves in the horizontal plane controlled by a tripod system. On the platform is a hexapod consisting of 6 electric linear actuators mounted. A vehicle body where the driver sits is attached on this hexapod platform. The body is in this case a Volvo V40. The tripod and hexapod system combined gives the total amount of nine degrees of freedom. The graphics are projected by three projectors on a panoramic screen giving a vertical field of view of 220 degrees.

The simulator gives Volvo Cars the opportunity to perform tests and evaluations of different vehicle systems that has not yet been built. This means that tuning and testing can be done in an earlier state in the development improving efficiency and refinement.

2.4.1 VI-CarRealTime software

VI-CarRealTime, CRT, is the chassis simulation software used in the moving base driving simulator. VI-CarRealTime may also be used for offline desktop simulations. The models in CRT is created by importing properties of the different systems from real measurements or from software like Adams car. In a previous Master thesis, [2], was Simulink used as a plug-in with CRT in order to simulate the electric power steering system of a Volvo V40. Running the EPS system in Simulink allows active features in the system to be considered in the CRT-model.

It is also possible to import edited manoeuvres and create own events in CRT. This allows for tests that were ran with a steering robot to be reproduced in VI-CarRealTime. Running the steering robot tests in CRT allows for validation of the the CRT-model as well as tuning of CRT-model to achieve the same vehicle characteristics as the measurements.

2.5 Kinematic And Compliance Measurement

A Kinematic And Compliance, K&C, measurements defines suspension and chassis motion for varying displacement and force inputs. Volvo Cars measures the K&C data on a Suspension Parameter

Measuring Machine, SPMM-rig, from Anthony Best Dynamics. A picture of the SPMM-rig can be seen in figure 2.12.

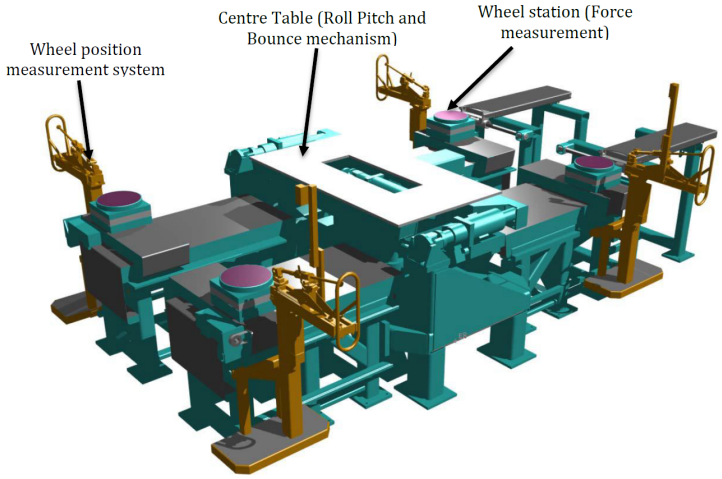

Figure 2.12: Image of the SPMM-rig

The chassis is connected to the centre table by clamps in the sills. The centre table can induce roll, pitch and heave motions onto the chassis. Each wheel is placed on top of a movable wheel station containing four load cells. The wheel stations are equipped with actuators that allows the platforms to move in a horizontal plane as well as rotation around the vertical axis. The wheel stations can either be locked in position or float which means that the forces in the horizontal plane is equal to zero. Measuring arms are mounted on the wheel hubs which measures the wheel hub displacement and angles. A steering robot is used during K&C measurement. The steering robot can input and measure steering wheel torque as well as steering wheel angle.

2.6 Steering And Handling DNA

Steering and Handling DNA is an objective measurement and post processing method that characterises a certain vehicle from a steering and a handling perspective. The steering and handling DNA consists of a number of manoeuvres respectively and is designed in such way that properties of the system can be evaluated and a rating is set depending on the result. The vehicle equipped with a steering robot as well as a throttle controller during the manoeuvres in order to increase the reproducibility. The vehicle is also equipped with an Oxford IMU system which measures motion, position and orientation. Each manoeuvre is ran several times to study the deviation between each run and increase the accuracy when using the data.

2.7 Genetic Algorithm

Genetic algorithms are optimisation methods that iterates toward a solution based on natural selection [14]. The method is effective for non-linear or non-differentiable problems and it can also be useful for black-box problems. The method uses a defined population of individual solutions that is scored via a fitness function dependant on how well the solution performed. The fitness function will either be minimised of maximised to receive the best solution. The individual solutions that scored best via the fitness function will then be the ”parents” of a new population of individual solutions. The new population, or the next generation as it can be called, will have new individual solution created in three different ways called Elite Solutions, Crossover Solutions or Mutation Solutions.

Elite Solutions are solutions that gave the best result from the previous generation and is carried over without any change to the next generation [14]. Crossover solutions are solutions that is created by combining solutions that received a good scoring during the previous generation, so called parents. Some individual solutions are created from randomising a value within a parent to form a so called Mutation Solution. These Mutation Solutions are implemented to increase the change to find a better solution if the overall solutions has stagnated at a local maximum/minimum.

2.8 Root Mean Square Error

The Root Mean Square Error is a statistical tool to evaluate the difference of two different data set. The tool determines first the error for each data point against the corresponding reference data point. The error is then squared and a mean value is calculated. The square root is taken of the mean value which results in the final Root Mean Square Error , RMSE [6]. The RMSE value can be written as equation 2.37.

$$RMSE = \sqrt{\frac{\sum_{i=1}^{n} (\hat{y}_i - y_i)^2}{n}} \tag{2.37}$$

3 Methodology

In this chapter the method of the development of a competitor vehicle model is described. Two methods will be introduced and a short overview of each method will be shown. Measuring equipment and measurements used in this thesis will be explained followed by a walk-through of the method used to determine the tyre and steering characteristics.

3.1 Method Overview

Figure 3.1 describes an overview of the developed method of building a competitor vehicle model. The vehicle is measured in an SPMM-rig where the K&C data is received. The dampers are dismounted and measured in a damper-rig. The acquired data is used to build a vehicle model in CRT. The model created has no data of tyres nor a model that gives the correct steering feedback to the steering wheel. The steering system and the tyres are dependent on data collected from dynamic manoeuvres which is not achievable from the SPMM-rig.

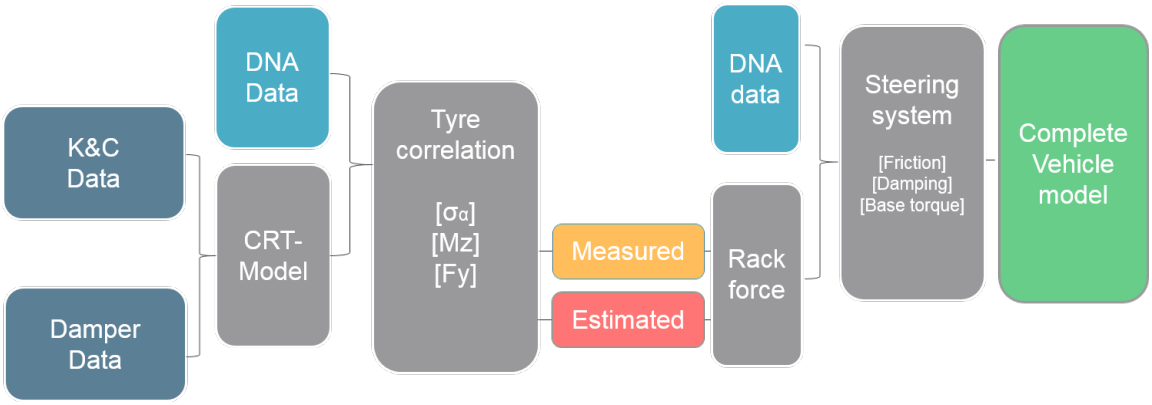

Figure 3.1: Overview over the methods developed

DNA-measurements using a steering robot and extra equipment such as tie-rod sensors are performed to gather dynamic data from a set of manoeuvres. The same manoeuvres are then ran in CRT. The tyres are tuned by starting from a Volvo Cars' standard tyre with known parameters which is tuned into a tyre that gives the same vehicle behaviour as the measurements shows. The lateral tyre parameters are assumed to be found when the vehicle model is achieving the same yaw rate and lateral acceleration as the measurements. The next step, tuning the aligning torque parameters, is performed in two different ways. One named Measurement Based Method and the other named Estimation Based Method. In the Measurement Based Method tie-rod force sensors are used and the aligning torque parameters of the Magic Tyre Formula are tuned against the measured tie-rod forces. The Estimation Based method is calculating the aligning torque using a Brush Model. With the tyres tuned by two different methods, the steering system can be derived in similar ways for the two methods. The steering wheel torque input is known from the DNA-measurements with steering robot and is compared with the rack force in order to estimate a relation. A look-up table is created giving a base torque output according to a given vehicle velocity and rack force. The base torque is influenced by friction and damping effects according to the steering wheel velocity. The damping and friction parameters are tuned to match corresponding DNA-manoeuvres.

3.2 Measurements

An essential part of this thesis was to define what parameters to be measured and what equipment was needed to do this. It was also important to determine which manoeuvres that should be performed to receive the measurements wanted. In this section the equipment and measuring methods are described as well as the test vehicle. Most of the tests and measurements were performed at Hällered proving ground.

3.2.1 Hällered Proving Ground

Volvo Cars' proving ground is located in Hällered. Here are fifteen tracks designed in order to cover most of the environments and situation a vehicle could experience during a life cycle. Endurance, NVH, corrosion, high speed driving, off road driving, start in slope, life time, handling ability as well as active safety and much more are tested here. The tracks that were used during this thesis was a skid pad with a radius of 40 m as well as a handling area with the dimensions 300 x 60 m. There are also a 4-post shake rig as well as a damper rig and a SPMM-rig located at Hällered. The workshop at sight enables modifications and evaluations of the vehicles.

3.2.2 Test Vehicle

Figure 3.2: Volvo XC90 mounted on the SPMM-rig

In this thesis was a Volvo XC90 used for data collection, figure 3.2. The reason for using a Volvo vehicle instead of a competitor vehicle was that the method can be evaluated. The vehicle is equipped with electric power steering assist system, EPAS. The ratio between steering wheel angle and rack displacement in the vehicle is constant except for the effects of the universal joints in the steering column. The Volvo XC90 used was equipped with the Volvo T6 engine and all wheel drive. The vehicle has a passive chassis which means that no air springs or active dampers were equipped. The total curb weight of the vehicle was 2050 kg and the maximum weight was 2750 kg.

3.2.3 Measuring Equipment

This thesis aims to find a method that with only small deviations from today's standard measurements still manages to create a vehicle model of a competitor vehicle. Three levels of equipment were therefore introduced in order to evaluate what was needed in order to achieve high quality data and finally a well performing vehicle model. The first level was most similar to the standard equipment used during K&C and DNA-measurements. The first equipment level was used for the Estimation

Based Method. It needs to be combined with a physical tyre model to be able to receive the aligning torque tyre parameters. The second equipment level was used for the Measurement Based Method and contained tie-rod sensors additional to the standard measuring equipment. The third equipment level was planned as a reference level in order to validate the vehicle model created from the two different methods.

Estimation Based Method Equipment

The Estimation Based Method was equipped with the standard measuring equipment including a steering robot and an oxford IMU which was measuring the vehicle motion, figure 3.3. A controller mounted on the throttle was also included in the standard measuring equipment which allows for longitudinal velocity and acceleration control.

Figure 3.3: Steering robot mounted in the test vehicle

Measurement Based Method Equipment

The Measurement Based Method uses the instrumentation from the standard measuring method but with the addition of tie-rod force sensors. The geometry of the steering system needs to be measured which can be done with the use of a coordinate measuring machine. What needs to be measured are the coordinates of the outer tie-rod ball joint and the inner tie-rod ball joint in relation to the wheel hub centre following the ISO coordinate system. With the coordinates of the ball joints the length of the tie-rod can be derived as well as the initial angle between the steering rack and the tie-rod assuming the steering rack is mounted along the y-axis. The angle between the outer ball joint and x-axis would also need to be measured to determine a more accurate change of angle between the steering rack and tie-rod when steering. In this thesis was only planar motion of the tie-rod considered which result in that the z-coordinate is not studied.

Figure 3.4: Tie-rod with strain gauge sensor mounted

The tie-rod sensors used are made by the department of Finmekanik at Volvo Cars Torslanda. They consist of tie-rods with strain gauge sensors attached which are calibrated before being used. Similar sensors can be produced if a competitor vehicle is to be measured. The original tie-rods are replaced with the calibrated ones with strain gauge sensors during the test. Changing the tie-rods was done in less than one hour.

Reference Level Equipment

The reference level has the highest level of instrumentation. The reference level is supposed to evaluate the vehicle model and the measurements performed for the two different methods. It uses the standard measuring equipment with addition of tie-rod sensors and an optical wheel angle measurement system added. It also uses measuring wheels in order to achieve wheel forces to compare with the CRT-model. These equipments were not available during the span of this thesis resulting in that the reference level was not performed.

3.2.4 Kinematics and Compliance Test

Standard K&C measurements were carried out on the SPMM-rig. Compliance measurements at two additional ride height levels were also performed to receive information about how the compliance changes against normal load. A steering wheel torque sweep test was introduced. The test had locked wheel stations and a slowly increasing steering wheel torque was applied until the maximum force allowed on the wheel stations were received. The wheels should be kept in the straight forward position during the torque sweep. The steering wheel torque sweep test can be used to derive the compliance in the steering system by analysing torque applied at the steering wheel versus the steering wheel displacement.

Rack displacement to steering wheel angle relation was measured on the K&C-rig. This was done by using a wire potentiometer attached to the joint between the tie-rod and steering rack. This was performed with the vehicle lifted and one of the front wheel dismounted in order to reach the essential components. The setup can be seen in figure 3.5. The steering robot was set to slowly rotate the steering wheel from -200 degrees to +200 degrees while the corresponding rack displacement was captured. This relation was used to compute the rack displacement for the dynamic events.

Figure 3.5: Rack travel versus steering wheel angle measurement

3.2.5 Handling And Steering DNA

The following sections describe the objective manoeuvres used for data collection. They are based on standard manoeuvres but are also complemented with additional load cases.

Constant Radius

Tyres changes its characteristics depending on the normal load. The Constant Radius manoeuvre was therefore ran with two different vehicle load setups to receive a broader normal load span on the tyres and from that be able to determine the normal load dependency more accurately. The first vehicle load setup corresponded to curb weight of the vehicle with two persons seated in the front of the vehicle each weighing 70 kg, also called curb+2. The second vehicle load setup corresponded to the maximum weight of the vehicle where the additional weight was distributed in the rear seat and in the trunk of the vehicle. Tyre pressure was kept constant for the different vehicle loads to avoid the effect of tyre pressure to affect the result.

High G Swept Steer and On Centre

The HSS and OC manoeuvres were found to be suitable for estimation of the steering assist system. These manoeuvres were therefore wanted for an even spaced velocity interval to be able to capture velocity dependent variables in the steering assist system. Different frequencies and lateral accelerations was also wanted for the OC manoeuvre to study the steering assist system for different scenarios. The wanted manoeuvres are presented in table 3.1.

Table 3.1: Additional HSS and OC manoeuvres performed with the test vehicle

Manoeuvre type	***Frequency, Hz***	***Lateral acceleration, g***	***Vehicle Velocities, km/h***
On Centre	0.2	0.2, 0.4	40, 60, 80, 100
On Centre	0.7	0.4	40, 60, 80, 100
High g Swept Steer	-	-	40, 60, 80, 100

3.2.6 Damper Measurements

All four dampers of the test vehicle were dismounted and measured following a standard test procedure in a damper rig acquiring the dampers' force-velocity dependency. This data was then imported to

the vehicle model created in CRT. A compression ratio between damper motion and vertical wheel movement was also needed. This can be done on the K&C-rig by measuring the damper travel and vertical wheel displacement during a heave motion.

3.3 Vehicle Model

The vehicle model was created in CRT by using the vehicle model wizard and K&C data from the SPMM-rig. This method is described more in detail in appendix B. The CRT-model is based on look-up tables created from the K&C measurements and damper measurements. The steering wheel angle for the DNA data was set as an input parameter to the CRT-model to ensure that the CRT-model would have the same steering as the DNA manoeuvre. This also meant that the relationship between the steering wheel angle and the road wheel angle needs to be determined with high accuracy to achieve a good correlation between the CRT-model and the DNA data. The ratio between the steering wheel angle and the road wheel angle was received from the standard K&C measurements. The steering column compliance can be derived from the added steering wheel torque sweep measurement by studying how the steering wheel angle changes when steering wheel torque is applied and the wheels are kept stationary.

3.4 Tyre Modelling

Tyre characteristics is usually determined by mounting tyres in a test rig and measure forces and moments during certain normal load and side slip sweeps. This is not something Volvo Cars do but instead the tyres need to be sent to an external test facility. Due to limitations in time and cost it is not possible to include this within the scope of the developed method. An other way to measure the tyre characteristics is by mounting measuring rims and high-speed cameras to measure forces, moments and wheel angles. However the availability of such measuring equipment is limited and therefore such a setup can not be used for every competitor vehicle. Still, such a method has been developed within Volvo Cars using measuring rims and high-speed cameras and can therefore be seen as an option in certain scenarios when the accuracy of the tyre characteristics is very important.

With the delimitation stated for this thesis it was determined that the tyres should be re-parametrised by using a known Volvo Cars tyre model as reference. The benefit of this is that not all variables need to be determined to receive a complete tyre data sheet. The longitudinal and combined characteristics, that will not be considered in this thesis, can be taken directly from the known Volvo Cars tyre. The camber characteristics will not be tuned and the default values for the tyre is kept. The shift factors has a high uncertainty and can differs from tyre to tyre within the same type. The shift factors were therefore set to zero to give equal error to positive as negative shift. The lateral force and aligning moment characteristics can be tuned by measuring data to fit the competitor vehicle tyres. The known tyre that will be used as a starting point will be determined by which tyre that has the closest tyre characteristics to the competitor tyre. This can be found by running the same manoeuvre as the DNA data in CRT for different tyres and study for instance which has the closest lateral acceleration curve to the DNA data. The tyre data of the known tyres are based on the Magic Tyre Formula.

3.4.1 Lateral Force

The Magic Tyre Formula factors that was determined to be tuned was peak factor, cornering stiffness factor and curvature factor. The peak factor was tuned due to its influence of the maximum force that can be achieved by the tyre. The cornering stiffness factor determines the slope in the linear tyre region and was tuned due to its high influence on the vehicle characteristics. To receive where

the peak lateral force occur and how the tyre acts between the linear regions and the peak value the curvature factor was tuned.

The Magic Tyre Formula factors was tuned by studying a Constant Radius manoeuvre. The Constant Radius manoeuvre was ran with two different vehicle load setups as explained in previous section 3.2.5. All the factors were tuned by the use of a Genetic Algorithm where the fitness function was the sum of the RMSE value between the simulated data and the measurements for the two different vehicle load setups.

To achieve the same manoeuvre in CRT as in the DNA data the steering wheel angle recorded in the DNA data was used as the steering input to the CRT-model. This was possible through Co-simulation between CRT and Simulink. An idealised velocity profile was used as reference speed for the virtual driver model in CRT.

Linear Region

The linear region was assumed to be below 40% of the maximum peak lateral acceleration achieved in the Constant Radius manoeuvre. The cornering stiffness factor can be expressed as the inclination of the linear region of the tyre and was the first tyre factor to be tuned. The factor was tuned against both lateral acceleration and yaw rate to achieve both the right total lateral force and the right balance between the front and the rear tyres. The tyre parameters were determined by which combination resulted in the lowest RMSE value for both the lateral acceleration and yaw rate combined.

Non-linear Region

The non-linear region was defined as 40% of peak lateral acceleration up to the peak of lateral acceleration. For the non-linear region the peak factor and the curvature factor was tuned simultaneously. The factors were tuned in similar ways as for the cornering stiffness factor against lateral acceleration and yaw rate. The RMSE value was used as an evaluation tool for determining the optimal parameters.

Relaxation length

In tyre test rigs the relaxation length is determined by introduce the tyre to a step steer at a certain velocity and measure the time before the forces achieve 63% of the steady state values. When measuring the complete vehicle a similar approach can not be done. This is due to when measuring a tyre on a test rig the side slip angle is induced instantly while when doing a complete vehicle test the side slip angle will not be induced instantly. This will result in that the relaxation length would be larger and correlate to the complete vehicle relaxation length rather then the tyres. The relaxation length was therefore derived from cornering stiffness and lateral stiffness, according to equation 2.11. The lateral stiffness was measured at each bounce level in the K&C-rig due to it is dependent of normal load. A function for the lateral stiffness was derived by curve fit the data points received from the K&C measurements.

3.4.2 Aligning Torque

Aligning torque is a key factor of what the driver feel in the steering wheel. The tuning of the aligning torque was evaluated in two different ways. The Measurement Based Method has strain gauge sensors added on the tie-rods of the vehicle. The aligning torque can then be tuned by matching the simulated tie-rod forces against the tie-rod forces received from the DNA tests. The benefit of this method was that the aligning torque can be tuned against DNA data and the tyres and steering system can be decoupled from each other. The second method, Estimation Based Method, was based on using the same measuring setup as for a normal DNA test and instead of tuning the aligning torque it was calculated by using a physical tyre model. The benefit of this method is that no extra measuring

equipment needs to be added and is therefore quick to implement. The drawback with the Estimation Based Method is that the accuracy of a physical model is lower and that the tyres and steering system can not be decoupled. However with the main purpose to achieve a representative model on full vehicle level and not on a component level some errors that can be introduced in the tyres could be adjusted in the steering system and still result in a well correlated vehicle model.

Measurement Based Method

This method tunes the tyres aligning torque factors by tuning simulated rack force in CRT to receive the same value as derived rack force from measurements. The steering geometry needs to be determined to be able to correlate the measured tie-rod force to steering rack force. The angle between the steering rack and the tie-rod will also change due to steering wheel angle and bounce. For simplicity the bounce effects are neglected. The steering geometry can be visualised in a top view in figure 3.6.

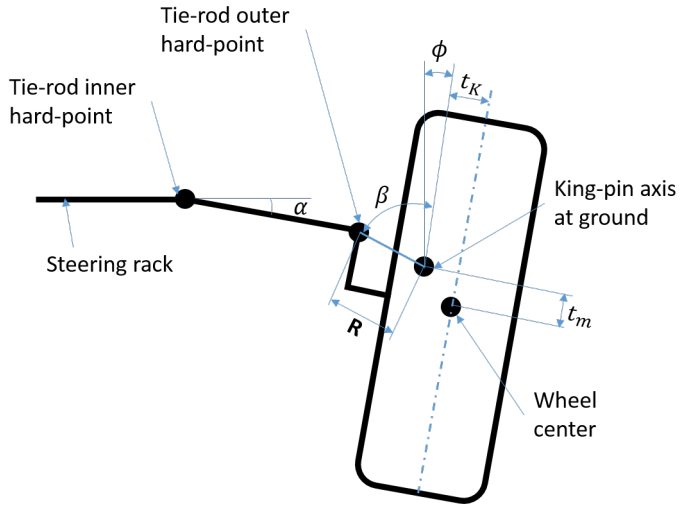

Figure 3.6: Overview of the steering geometry

where R is the radius of the King-pin axis at ground level to the outer tie-rod hard-point, β is a constant angle between the radius R and the longitudinal direction of the tyre. t_m is the mechanical trail and t_K is the King-pin offset. The radius R can be derived from studying figure 3.7 and see the displacement as a circle arc which result in $R = \Delta x/\Delta\phi$. The ratio which defines R can be execrated from K&C measurement. α is the angle between the tie-rod and the steering rack and can be expressed as equation 3.1.

$$\alpha = \alpha_0 + \Delta\alpha \tag{3.1}$$

where α_0 is the initial angle between the tie-rod and the steering rack when the tyres are pointing straight forward. $\Delta\alpha$ determines the change in angle due to steering input. Figure 3.7 shows the steering geometry with a steering rack displacement of Δx.

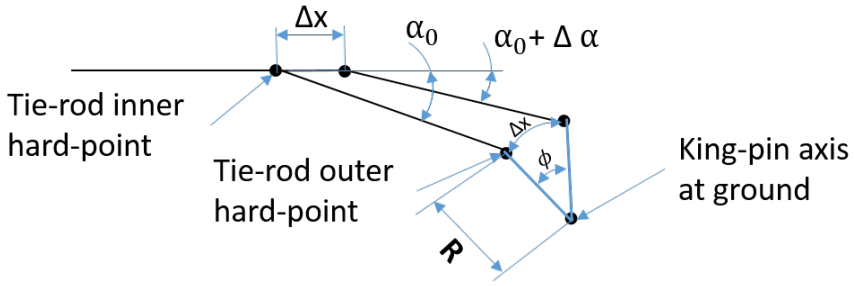

Figure 3.7: The steering geometry with a rack displacement of Δx

The change in angle can be expressed by studying how the outer tie-rod hard-point rotates along a circle arc as can be seen figure 3.7. The expression of the angle change can be seen in equation 3.2.

$$\Delta\alpha = \text{acos} \cdot \left(1 - \frac{r^2}{2 \cdot L^2} \cdot (1 + \cos^2(\beta) - 2 \cdot \cos^2(\phi))\right) \tag{3.2}$$

With the initial angle and the change of angle due to steer input derived from measurements the lateral tie-rod force component can be expressed as equation 3.3.

$$F_{tierod,y} = F_{tierod} \cdot \cos(\alpha_0 + \Delta\alpha) \tag{3.3}$$

An overview over the forces acting on the steering rack can be seen in figure 3.8.

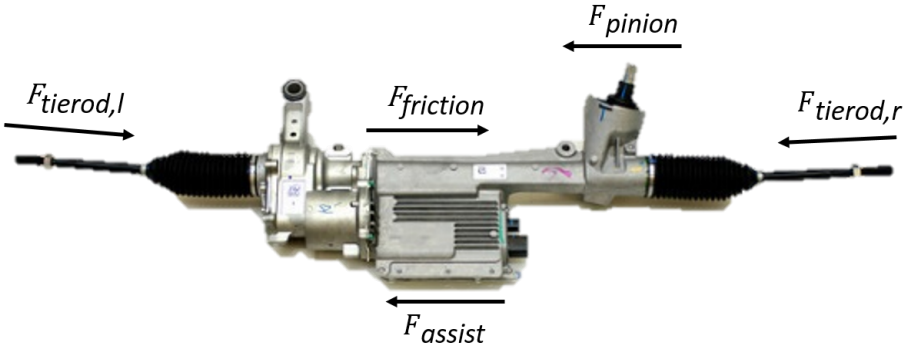

Figure 3.8: Free body diagram over a steering system

Newtons second law can be stated for the steering rack in y-direction as equation 3.4 shows.

$$m_{rack} \cdot a = F_{pinion} + F_{assist} - F_{friction} - F_{tierod,y,l} + F_{tierod,y,r} \tag{3.4}$$

where m_{rack} is the mass of the steering rack, F_{pinion} is the force applied from the steering pinion and F_{assist} is the force received from the steering assist system. The steering rack is stationary in the Constant Radius manoeuvre which is used when tuning the tyre characteristics with the exception of small compensations due to understeer of oversteer. This results in that both the friction in the system as well as the acceleration will have small effects on the system and can be neglected. Further is also the mass of the steering rack assumed zero, $m_{rack} = 0$. This results in that equation 3.4 can be written as equation 3.5.

$$F_{tierod,y,l} - F_{tierod,y,r} = F_{pinion} + F_{assist} = F_{steering} \tag{3.5}$$

where $F_{steering}$ is the total force from the steering system, $F_{pinion} + F_{assist}$, which is equal to the sum of the tie-rod forces. The $F_{steering}$ force can be seen as the rack force from the measurements. The rack force receive from the CRT-model will be tuned to achieve the same force as $F_{steering}$ by tuning the aligning torque parameters.

Estimation Based Method

If the tie-rod forces is not measured the aligning torque can not be tuned in similar ways as mentioned in Measurement Based Method. This is due to it has nothing it can be tune against. The steering wheel torque can not be used due to that the steering assist is unknown. Therefore a physical tyre model was used to create a connection between the tuned lateral force and the aligning torque, a Brush Tyre Model was used for this purpose. The physical parameters for the aligning torque stated in the Brush Model can be derived from the tuned lateral force parameters. The peak factor, the cornering stiffness factor and the contact patch length was used to determine the physical properties of the Brush Model. The contact patch length, L, can be seen in figure 3.9 and was derived by equation 3.6.

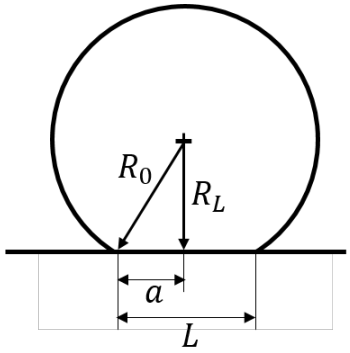

Figure 3.9: Visualisation of unloaded and compressed radius of a tyre

$$L = 2 \cdot a = 2 \cdot \sqrt{R_0^2 - R_L^2} \tag{3.6}$$

where R_0 is the unloaded radius of the tyre and R_L is the compressed radius of the tyre which is derived by equation 3.7.

$$R_L = R_0 - \frac{F_{z,wheel}}{C_{stiff,z}} \tag{3.7}$$

Where $F_{z,wheel}$ is the normal load on the tyre and $C_{stiff,z}$ is the vertical stiffness of the tyre. The vertical stiffness was derived from K&C measurements.

With the contact patch determined and the cornering stiffness and peak factor taken from the tuned parameters the equation for aligning torque 2.26 can be rewritten as equation 3.8:

$$M_z(\alpha) = \begin{cases} -D \cdot a \cdot \Theta_y \cdot \sigma_y \left(1 - 3|\Theta_y \sigma_y| + 3(\Theta_y \sigma_y)^2 - |\Theta_y \sigma_y|^3\right) & When\ |\alpha| \leq \alpha_{sl} \\ 0 & When\ |\alpha| > \alpha_{sl} \end{cases} \tag{3.8}$$

where

$$\Theta_y = \frac{C_{f\alpha}}{D \cdot 3} \tag{3.9}$$

$$\sigma_y = \tan(\alpha) \tag{3.10}$$

$$\alpha_{sl} = \frac{1}{\Theta_y} \tag{3.11}$$

The calculated aligning torque is then used to tune the Magic Tyre Formula variables for the aligning torque with the use of a Genetic Algorithm in the same ways as for the Measurement Based Method.

3.5 Steering Model

In the driving simulator, the steering wheel angle is used as an input from the driver to the steering system. The steering system outputs a torque feedback to the driver depending on the vehicle state. The torque feedback system was determined to be a function of rack force, vehicle velocity and steering wheel velocity. These variables were chosen due to that they are often used in today's steering systems. The forces acting in the steering system derives from equation 3.4 and 3.5. With the assumption of neglected steering rack mass the resulting equation can be seen in equation 3.12.

$$F_{pinion} = F_{steering} - F_{assist} + F_{friction} \tag{3.12}$$

The assist force F_{assist} can be expanded into equation 3.13 by dividing the total assist force into motor force, friction and damping. The motor force in this thesis corresponds to the steady state force, without friction, that is applied from the steering assist system. The friction and damping are introduced to increase the tuning possibilities of the steering assist system.

$$F_{assist} = F_{motor} - F_{mfric} - F_{damping} \tag{3.13}$$

The F_{mfric} is the friction added by the steering assist system. The different friction in the steering system can not be derived separately which results in that the total friction, $F_{fricTot}$, in the steering system needs to be used and is expressed as equation 3.14.

$$F_{fricTot} = F_{friction} + F_{mfric} \tag{3.14}$$

One of the interesting variables in the steering system is the difference between $F_{steering}$ and F_{motor} and is called base force, F_{base}. The base force can be seen in equation 3.15.

$$F_{base} = F_{steering} - F_{motor} \tag{3.15}$$

Inserting equation 3.13, 3.14 and 3.15 into equation 3.12 results in equation 3.16.

$$F_{pinion} = F_{fricTot} + F_{damping} + F_{base} \tag{3.16}$$

Equation 3.16 represents the steering algorithm and consist of three main components: base force, friction and damping. The steering wheel torque can be seen as F_{pinion} times the ratio between steering wheel angle and rack travel.

3.5.1 Steering Feedback Model

The steering feedback model was built in Simulink, depicted in figure 3.10. The system consists of a CRT-block with a vehicle model and a steering feedback algorithm block. The vehicle model contains the defined velocity and acceleration for the studied manoeuvre. Rack force, longitudinal vehicle velocity and steering wheel velocity are defined as outputs from the vehicle model. These signals goes into the steering feedback, marked with a green frame. The topology of this block can be seen in appendix C. Damping and friction effects are calculated as functions of steering wheel velocity and added to the base torque as described by equation 3.16. The sum of these three is then defined as the output steering wheel torque to the driver.

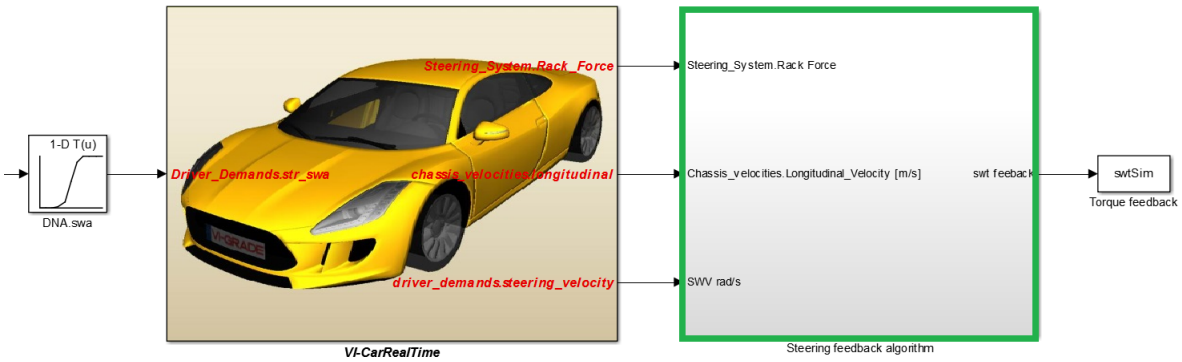

Figure 3.10: Topology of steering system in Simulink

The base torque output is mainly valid for an increasing steering wheel angle. When increasing the steering wheel angle the driver needs to overtake effects like aligning torque, friction and damping. The aligning torque aims to keep the wheels straight. The friction and damping are always counteracting the motion and will work against the aligning torque when decreasing the steering wheel angle. This means that less torque is needed from the driver when decreasing the steering wheel angle compared against increasing it. This results in an hysteresis which is not accounted by the base torque table but is simulated by adding friction and damping effects to the system.

3.5.2 Base Torque Table

The base torque is defined as F_{base}, from equation 3.15, times the ratio between the steering wheel angle and rack travel. The algorithm controlling the force applied by the assist motor of the test vehicle is not known which was why the base torque table was introduced. Base torque is acquired by calculating the difference between steering wheel torque and rack force during a HSS manoeuvre with friction and damping contribution subtracted. The HSS manoeuvre was performed at 40, 60, 80 and 100 km/h. For each run was a curve fit of the rack force versus steering wheel torque created using the built in polyfit-tool in Matlab. From this was the friction and damping subtracted resulting in a base torque curve. To avoid unrealistically high rack forces outside the measured region, no extrapolation was used. The base torque will instead become constant outside the measured region. The created curve was mirrored about the x-axis to cover negative rack forces, corresponding to a turn in the opposite direction. In order to make the transition between the positive and negative torque smooth the transition equations 3.17 and 3.18 were used, where $F_{steering}$ is the rack force and κ is a curvature factor. The curvature factor regulates the transition between the polyfitted function and its mirrored function. The merging of the two functions results in one curve representing the

base torque for a certain velocity.

$$\sigma = \frac{1}{1 + e^{-F_{steering}/\kappa}} \tag{3.17}$$

$$y_{tot} = (1 - \sigma) \cdot y_1 + \sigma \cdot y2 \tag{3.18}$$

Measurement Based Method

The rack force was derived as described earlier in 3.4.2. The total rack force was put in relation with the measured steering wheel torque and a base torque table was produced.

Estimation Based Method

The built CRT-model, with the estimated tyre parameters imported, simulates rack force in a Co-simulation between CRT-model and Simulink as described in figure 3.11. The vehicle model used in the CRT-block has a pre-defined velocity profile equivalent to the DNA-manoeuvre. This means that the steering wheel angle measured in the DNA test was the only input needed for this model in Simulink. The total rack force was used as an output from the simulation and is marked with a red frame in figure 3.11. The total rack force is exported from the Simulink model and used to create a base torque look-up table.

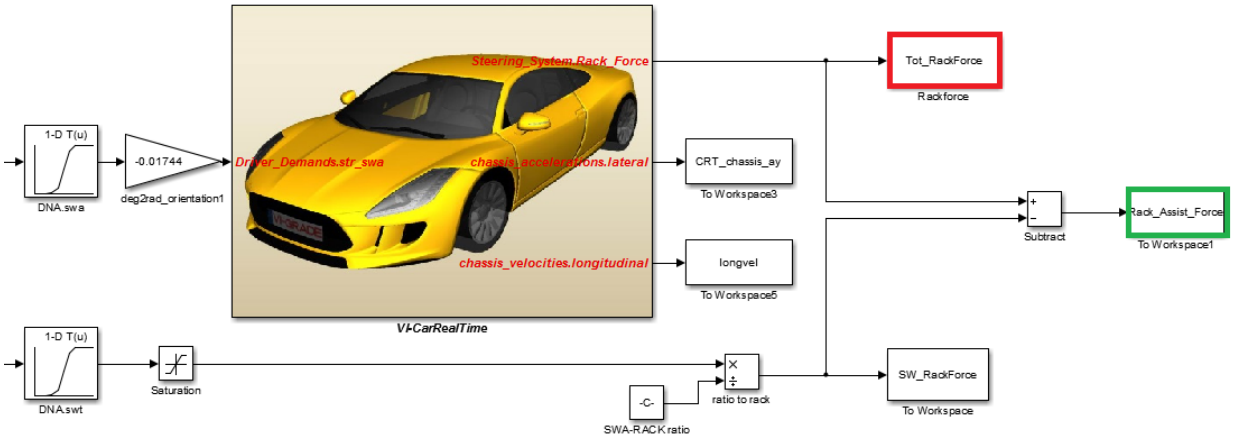

Figure 3.11: Simulink model for calculating the steering assist force

3.5.3 Damping

The damping coefficient was designed to be lower at high steering wheel velocities. The reason for a higher damping coefficient at low velocities was to match the measured torque during On Centre manoeuvres. However, to avoid overestimated damping torque during more transient manoeuvres the damping coefficient had to be decreased. The equation used to calculate the resulting damping coefficient, C_d, is seen in equation 3.19. By tuning the model for different manoeuvres, a highest, C_{max}, and lowest, C_{min}, value of damping coefficient as well as a curvature factor, κ, was decided. The maximum coefficient is meant to be used only at low steering velocities. The decided coefficients are multiplied with the steering wheel velocity which results in a damping torque.

$$C_d = ((C_{max} - C_{min}) * (e^{-\frac{swv}{\kappa}}) + C_{min}) \tag{3.19}$$

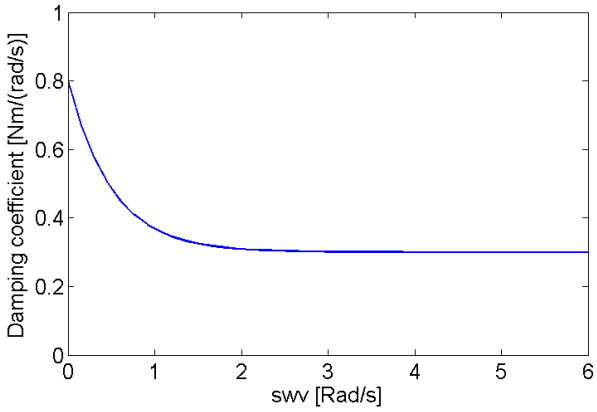

Figure 3.12: Damping torque vs steering wheel velocity for the steering system

3.5.4 Friction

The friction is always counteracting the steering motion. This results in a high risk for instability in the steering system caused by discontinuity when changing steering direction. The instability was avoided by having a continuous friction curve which passes through zero when the steering wheel velocities changes sign. The curve becomes constant when higher steering velocities are reached. The friction behaviour was shaped using the Magic Tyre Formula presented in equation 2.28. This formula was used to imitate stick slip friction by shaping a initial peak on the curve which corresponds for the extra torque required to release the system from stand still. This means that the friction will decrease to a lower constant value relative to the peak value when the system is in motion. An example of a friction curve is visualised in figure 3.13. The shape of the friction is constant for all simulations but the amplitude of it is tuned in the optimisation.

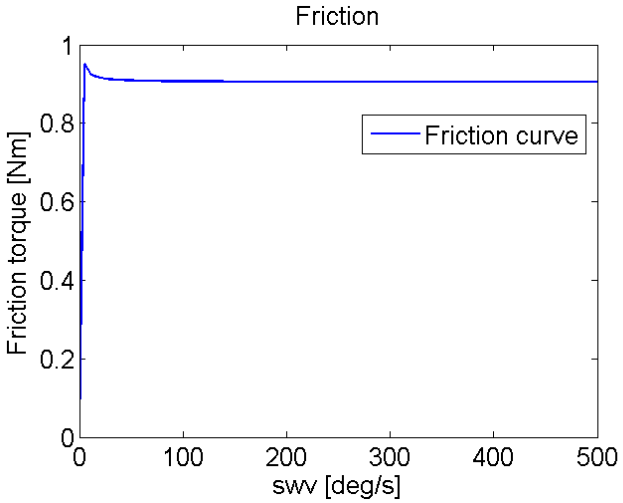

Figure 3.13: Friction curve for the steering system

3.5.5 Optimising Steering Parameters

The parameters in the steering system was tuned to give a simulated feedback torque that represent the measured torque. The steering model was tuned against specific manoeuvres and was ran against other manoeuvres to evaluate how well the steering system was captured. A Matlab script was created which imported a specific manoeuvre, ran CRT and exported the simulated rack forces.

From the simulated rack force was the steering wheel torque derived. The RMSE value between the simulated steering wheel torque and the measured steering wheel torque received from the DNA test was calculated using equation 2.37. The friction and damping parameters was optimised by minimising the RMSE value using "fmincon" in Matlab. The parameters optimised were C_{min}, C_{max}, κ and $friction$. Constraints was set in the "fmincon" optimiser in order to receive realistic values and shorten the simulation time. The optimisation flow is visualised by the orange arrow in figure 3.14.

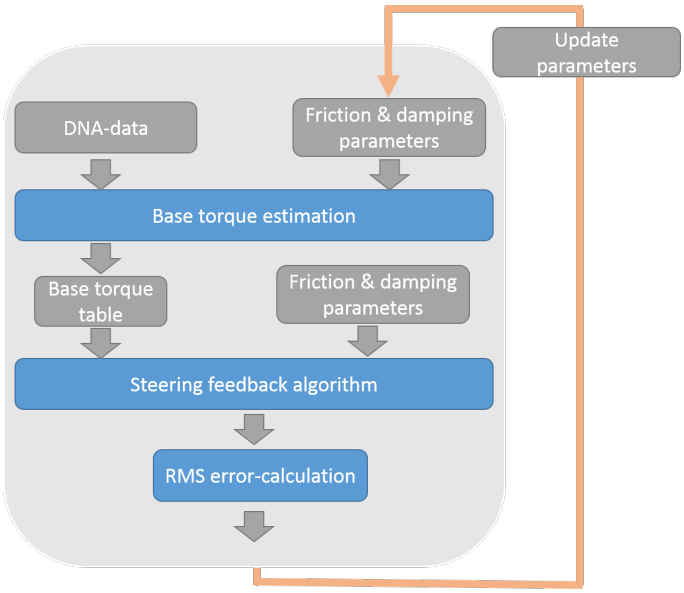

Figure 3.14: Flowchart representing the optimisation algorithm

Measurement Based Method

The tuning of the steering system with measured rack forces was performed in two ways. Firstly by studying the steering system independently by only using measured data from manoeuvres. This allowed the modelled steering system to be objectively evaluated as of an ideal vehicle model was achieved. The CRT-model was not needed in this simulation. The measured DNA-data was instead connected into the steering feedback algorithm marked with a green frame in figure 3.10.

The Measured Based Method can however not be used this way in the driving simulator. Even if measured rack forces was used when defining the base torque look-up table the rack forces into the steering feedback model will be given from the simulated vehicle model when running it in the driving simulator. Therefore, the result when combining the DNA measured look-up table with simulated rack forces is of higher interest when evaluating how well the full system performs. In this thesis, the damping and friction parameters were tuned when running the steering system independently for both the Measurement Based Method setups.

Estimation Based Method

The Estimation Based Method was performed only for a driving simulator setup due to that the steering system can not be evaluated independently following this method. The coupled steering and tyre system allows only for simulated rack forces to be used. The steering system used is presented in 3.10.

3.5.6 Simulator Implementation

The steering system was implemented into the simulator by replacing the CRT-block presented in figure 3.10 with outputs from the vehicle model of the simulator. The steering wheel torque output from the steering feedback model was sent to the steering wheel in the simulator. An additional block was added to the torque output in order to ensure that no high values was received that could harm the driver or damage the equipment if the steering system would fail.

3.6 Evaluation

The evaluation of the competitor vehicle models created was performed both objectively and subjectively. Objectively by comparing simulation data with measurements from different manoeuvres. The subjective evaluation was done by allowing a number of vehicle dynamics engineers drive the three models in the driving simulator. The first model tested was the already existing XC90 vehicle model together with the conventional steering system. The second model was the model created using the Estimation Based Method and the third model was created using the Measurement Based Method. The drivers were driving each model on two different tracks. Firstly was straight ahead controllability tested by driving on a three lane straight highway. The second track was "Handlingbana 2" which is a representation of a handling track at Hällered. The overall handling was evaluated on this track. The tracks were used to evaluate the vehicle model in different areas. The straight highway evaluates the vehicle behaviour around On Centre while "Handlingsbana 2" evaluates more transient driving.

4 Results

4.1 Vehicle Model

The vehicle model created in CRT showed high correlation against the K&C measurements used. Steering compliance in the steering column was thought to be received from the added torque sweep test on the K&C-rig. However the data received from the K&C-rig showed no consistent results and a possible reason could be that the tyres were sliding on the pads resulting in measuring errors. An alternative test would be to replace the tyres with rigid replacements to increase the accuracy of the steering column compliance. The steering column compliance was instead tuned manually by the use of tyre data from the same tyres as was mounted on the test vehicle during the DNA manoeuvres. With that tyre data inserted into the CRT-model the steering column compliance could be tuned against DNA data. The correct steering column compliance was assumed to be correct when the same lateral acceleration and yaw rate was received from the CRT-model as for the DNA data for a Constant Radius manoeuvre. It was found that an overestimation of the steering compliance could result in that the tyres could not achieve the same lateral acceleration and yaw rate as the DNA data. This is due to the optimum path, meaning the path the vehicle would follow with zero side slip angle or infinity high cornering stiffness, would have lower lateral acceleration and yaw rate than the DNA data. This would result in that the tyre tuning algorithm would tune the cornering stiffness to infinity without reaching the DNA data. For an underestimation of the steering compliance the tyre tuning would simply result in a too low cornering stiffness compared to the actual tyre data sheet. However the side slip angle would also increase compensation for the lower cornering stiffness which would result in the same lateral acceleration and yaw rate but the vehicle would follow a slightly different path. Due to that the steering compliance had to be tuned through simulations with the full vehicle model, other effects such as possible errors in the model itself could influence the steering compliance resulting in the received value could deviate from the actual compliance value. The tyre data could also influence the steering compliance due to that the tyre data is received from Flat-Track measurements while the manoeuvre used when tuning the compliance was performed on an other surface.

The steering geometry was not measured in this thesis resulting in that both β and α_0 was set to zero in equation 3.2 and 3.3 respectively. Both the angles should be small to optimise the steering capacity however due to packaging the angles can not be neglected in some cases. Therefore can a conversion error be induced if not the steering geometry is measured.

4.2 Tyre model

The CRT-model can not handle low speed manoeuvres which was a problem when studying a Constant Radius manoeuvre. The manoeuvre starts at 10 km/h and increases the longitudinal velocity slowly. It was found that the lower limit for longitudinal velocity of the CRT-model was at 30 km/h which resulted in that the model had to start when the Constant Radius manoeuvres had reached a velocity of 30 km/h. The CRT-model can have an initial steering wheel angle but the initial state of the vehicle can not be changed meaning that for instance lateral acceleration and yaw rate starts from zero. This meant that the CRT-model is not in the same vehicle state as the DNA data in the beginning of the manoeuvre. An initial overshoot of lateral acceleration and yaw rate can be seen in figure 4.1 and 4.2 which is a result of the difference in initial vehicle state. The beginning of the manoeuvre until the vehicle was stabilised was therefore not considered when tuning the tyres.

The tyres was first tuned to achieve the same lateral acceleration and yaw rate in the linear tyre regions of the DNA data for a Constant Radius manoeuvre. The tyre variable that was tuned was the cornering stiffness using a GA function. After the linear region was tuned the non-linear regions

was tuned against the same DNA data by influence the peak factor and the curvature factor. The result in lateral acceleration and yaw rate can be seen in figure 4.1 and 4.2 respectively. The figures shows the lateral acceleration and yaw rate from measurement as well as from the original tyre and the tuned tyre. The original tyre is the tyre that was chosen as the starting point for the tuning due to its similarities in tyre characteristics to the tyre mounted on the test vehicle. The measured data that are visible in the figures are a mean value of several data runs. The mean velocity profile for the DNA data was also the velocity profile used when determining the initial manoeuvre in CRT.

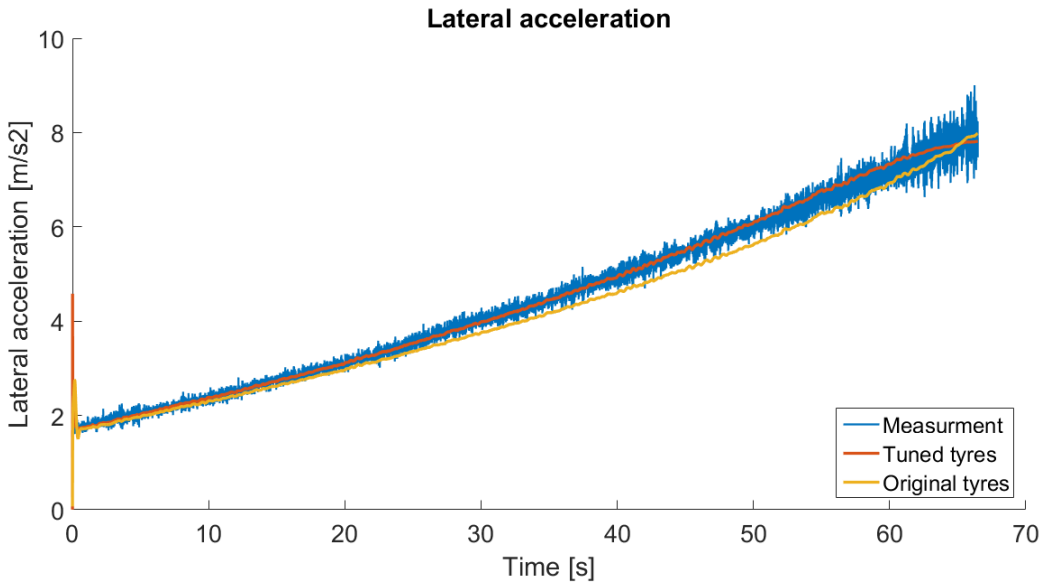

Figure 4.1: Comparison between tuned tyres,original tyres and measurements in lateral acceleration for a Constant Radius manoeuvre

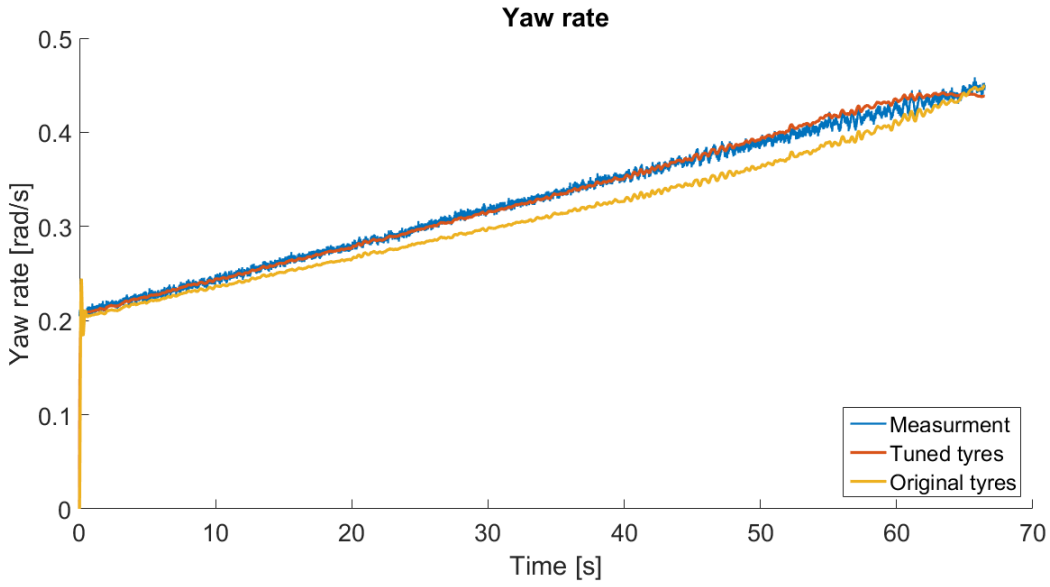

Figure 4.2: Comparison between tuned tyres,original tyres and measurements in yaw rate for a Constant Radius manoeuvre

One can see that the tuned tyre differs from the DNA data at higher lateral acceleration and yaw

rate. This can be due to that the camber effects has not been tuned in this thesis. The original tyre has a lower cornering stiffness and a still increasing peak friction at the end of the manoeuvre. The original tyre data is measured in a tyre test rig on a Flat-Trac surface where the friction is higher then where the DNA data is carried out. This explains the still increasing lateral acceleration at the end of the manoeuvre for the original tyre. Path projection was also extracted from the data and can be seen in figure 4.3. Here one can see that the tuned tyre follows the DNA data well. One can also see that the difference from the original tyre to the tuned tyre.

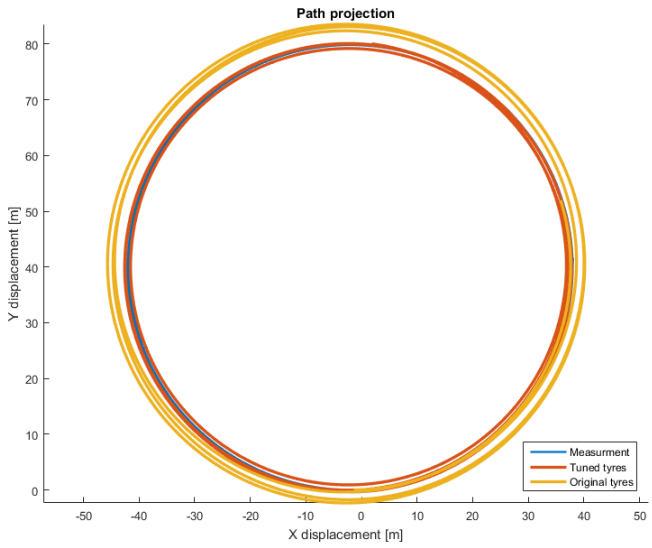

Figure 4.3: Comparison between tuned tyres,original tyres and measurements in Path projection for a Constant Radius manoeuvre

A important characteristic of the tyre is how the cornering stiffness is effected by the normal load. The normal load effect can be seen in figure 4.4.

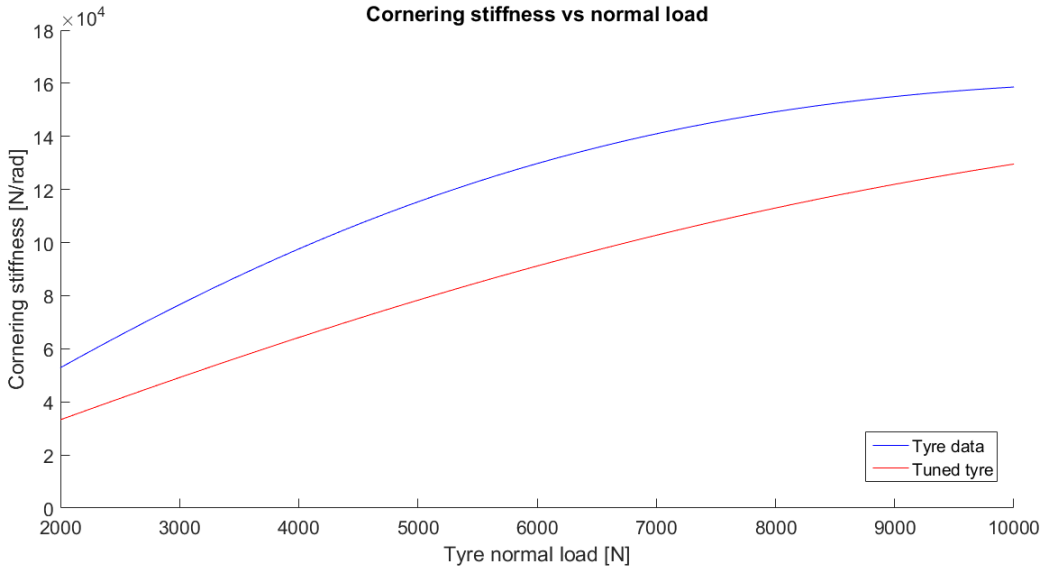

Figure 4.4: Cornering stiffness over normal load for tyre data of the same tyre type as used on the test vehicle and the tuned tyre

In figure 4.4 one can see that the cornering stiffness is lower for the tuned tyre. However, the different tyres are ran on different surfaces. This could influence the cornering stiffness not due to the difference in surface friction but rather due to the surface itself. Therefore can the tuned tyre show good correlation against measurements even thought when comparing against tyre data the tuned tyre show lower cornering stiffness.

To evaluate the tyre tuning the CRT-model was ran for other manoeuvres. The ones that was chosen for evaluation was a High g Swept Steer manoeuvre at 80 km/h to evaluate the non-linear and peak characteristics and two On Centre manoeuvres with a frequency of 0.2 Hz and 0.7 Hz respectively to capture more transient characteristics. Both On Centre manoeuvres had also a lateral acceleration of 0.4 g and longitudinal velocity of 80 km/h. The lateral acceleration, yaw rate and path projection of the HSS manoeuvre can be seen figure 4.5, 4.6 and 4.7 respectively.

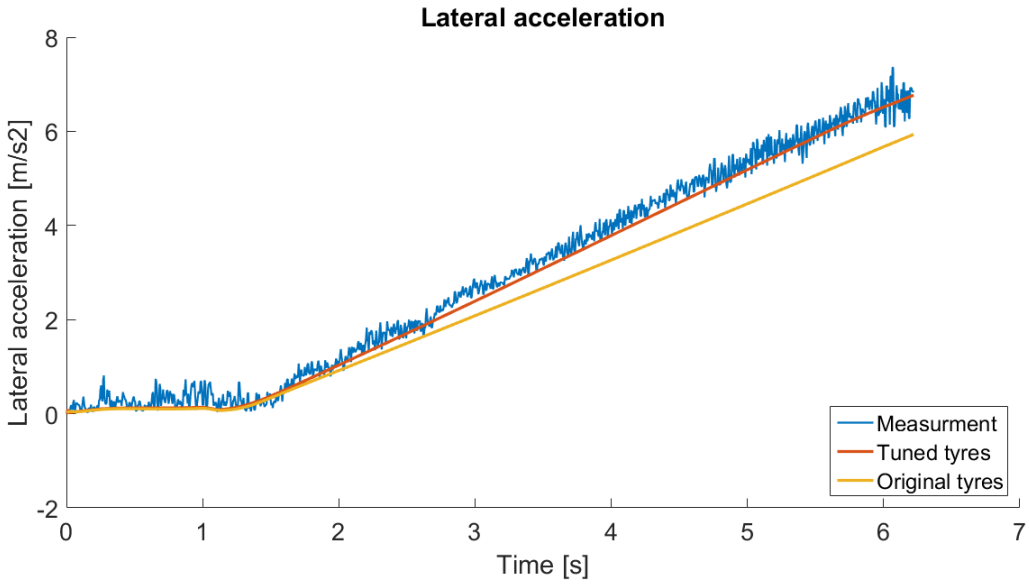

Figure 4.5: Comparison between tuned tyres,original tyres and measurements in lateral acceleration for a High g Swept Steer manoeuvre in 80 km/h

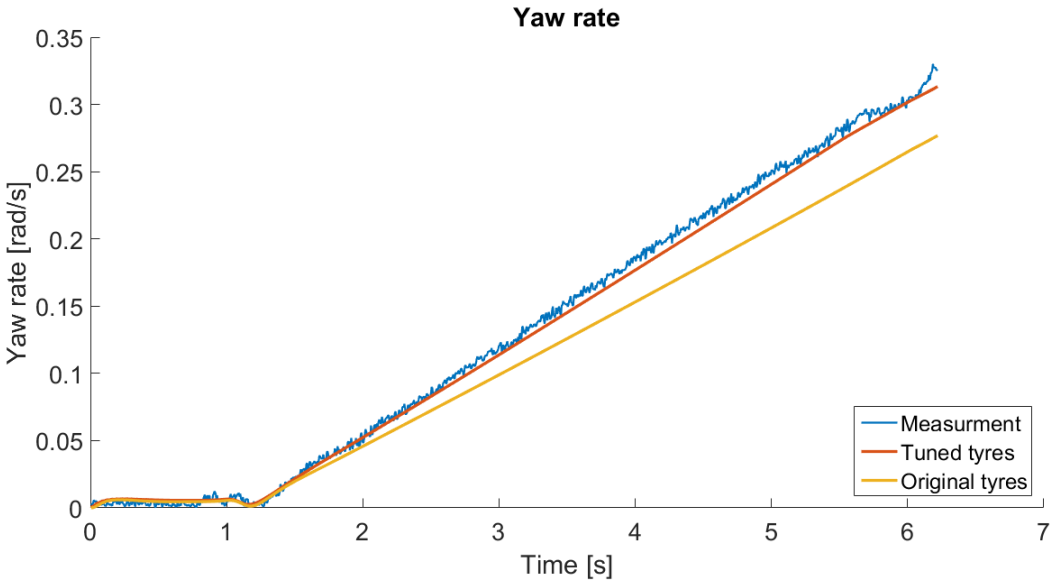

Figure 4.6: Comparison between tuned tyres,original tyres and measurements in yaw rate for a High g Swept Steer manoeuvre in 80 km/h

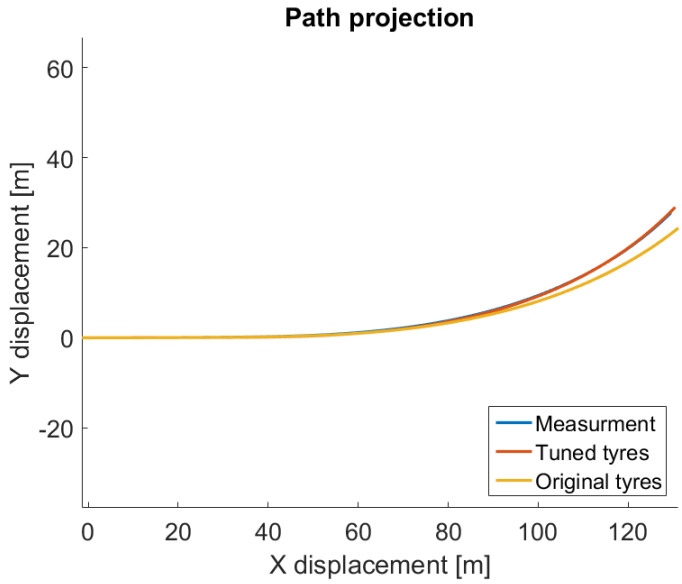

Figure 4.7: Comparison between tuned tyres,original tyres and measurements in path projection for a High g Swept Steer manoeuvre in 80 km/h

The slightly drop of lateral acceleration and yaw rate at the end of the manoeuvre can be explained by that one of the runs for the HSS manoeuvre had a small difference in longitudinal velocity and resulted in that it reached the maximum lateral acceleration after the other runs. The mean value of all the data runs resulted therefore in the slightly drop in the curves at the end of the manoeuvre. Studying the lateral acceleration, figure 4.5, and yaw rate, figure 4.6 , one can see that the tuned tyre follows the measured data well and that the original tyre had a lower lateral acceleration and the yaw rate overall. The path projection that can be seen in figure 4.7 shows that the CRT-model with the tuned tyres now follows the measured data.

The relaxation length was calculated by equation 2.11. The equation is not a true statement and

should be seen as an approximation. The influences of the calculated relaxation length can be seen as a contribution in phase shift when studying lateral acceleration and yaw rate for an On Centre manoeuvre, which can be seen in figure 4.8 and 4.9.

The results from the On Centre manoeuvre with a steering wheel frequency of 0.2 Hz are shown in figures 4.8 - 4.10. The figures shows of a high correlation between the measurements and the CRT-model with the tuned tyres.

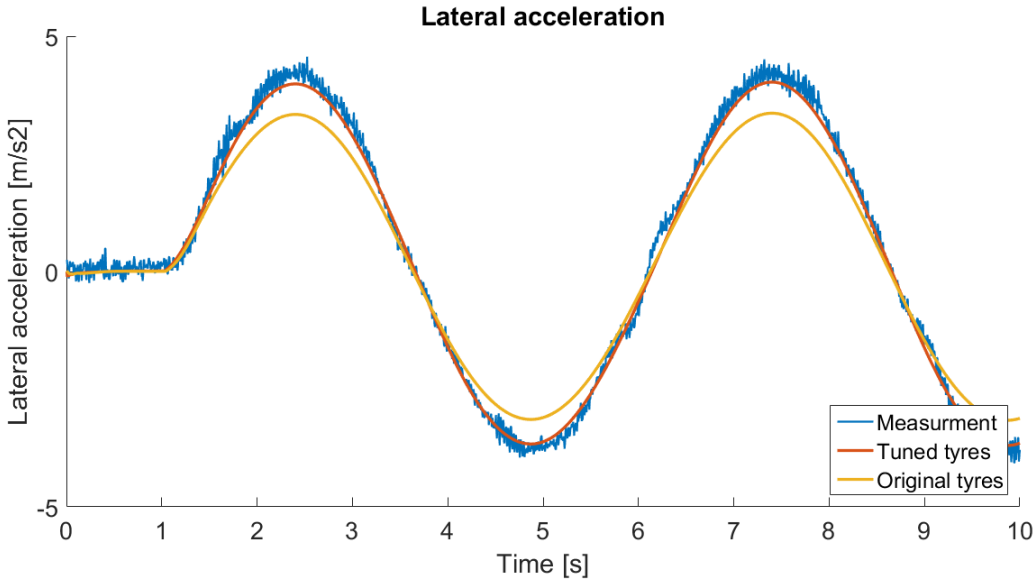

Figure 4.8: Comparison between tuned tyres,original tyres and measurements in lateral acceleration for an On Centre manoeuvre with a frequency of 0.2 Hz

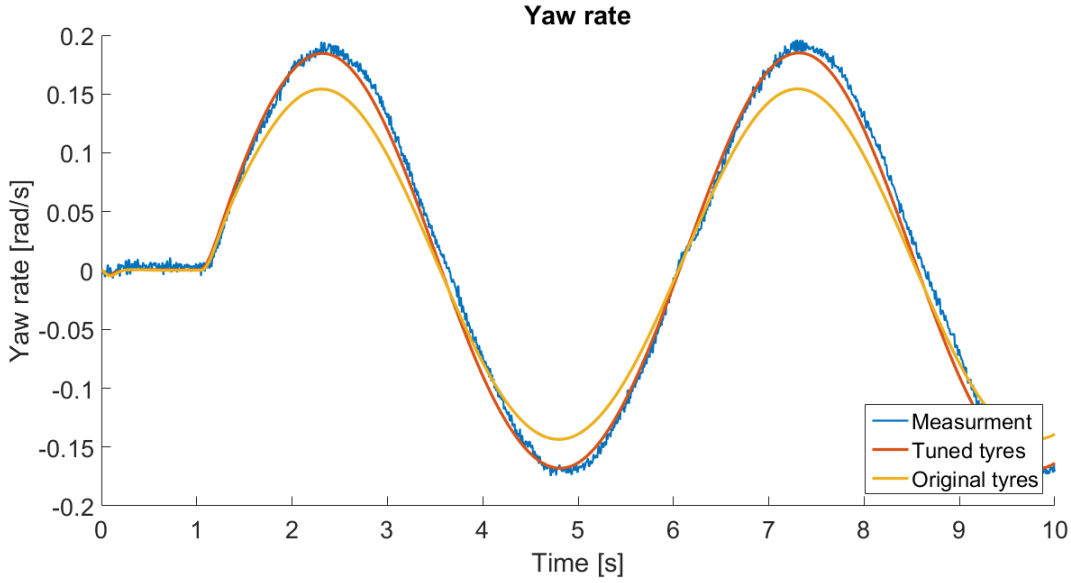

Figure 4.9: Comparison between tuned tyres,original tyres and measurements in yaw rate for an On Centre manoeuvre with a frequency of 0.2 Hz

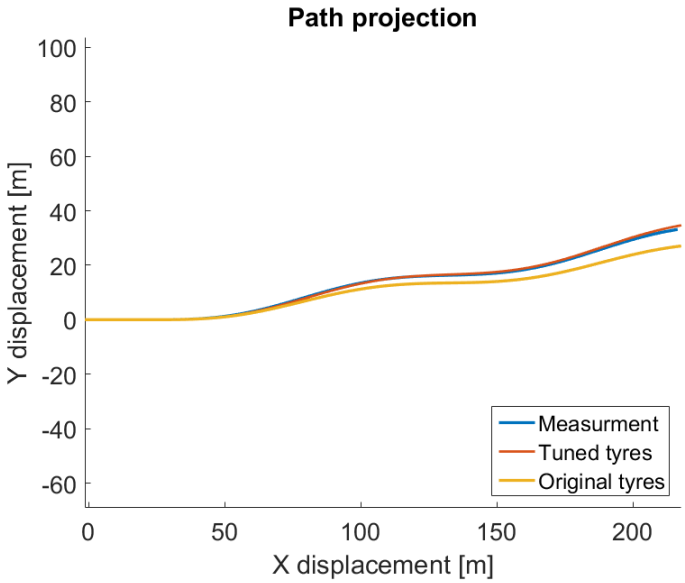

Figure 4.10: Comparison between tuned tyres,original tyres and measurements in path projection for an On Centre manoeuvre with a frequency of 0.2 Hz

Lateral acceleration, yaw rate and path projection for the On Centre manoeuvre with a steering wheel frequency of 0.7 Hz can be seen in figures 4.11-4.13. Here one can see that the lateral acceleration for the tuned tyre does not achieve the same magnitude as the measurement. The underestimation of lateral acceleration results also in that the CRT-model with tuned tyres does not follow the same path as the measurement. The yaw rate however shows high correlation between the measured data and the tuned tyres.

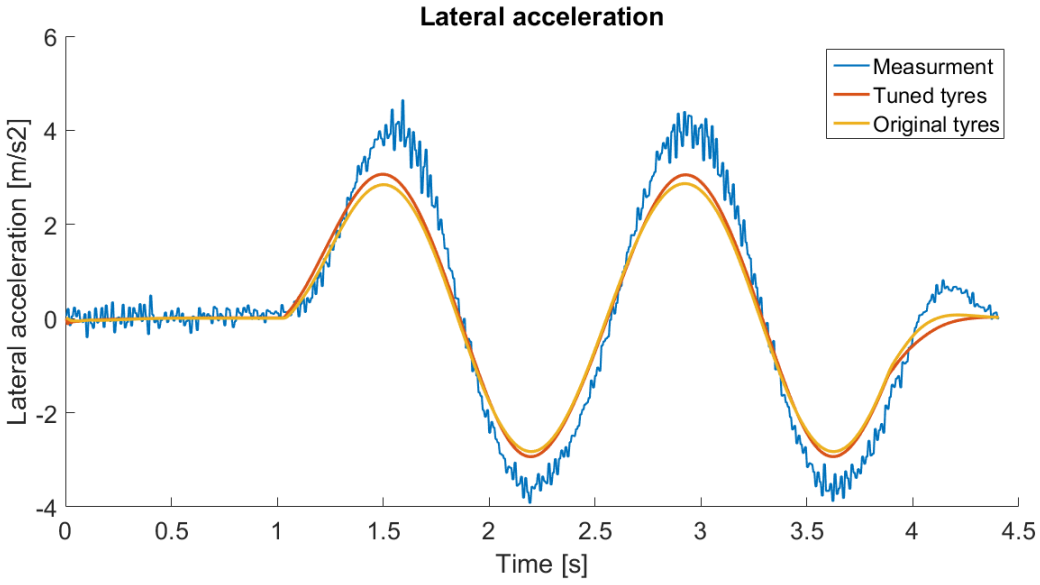

Figure 4.11: Comparison between tuned tyres,original tyres and measurements in lateral acceleration for an On Centre manoeuvre with a frequency of 0.7 Hz

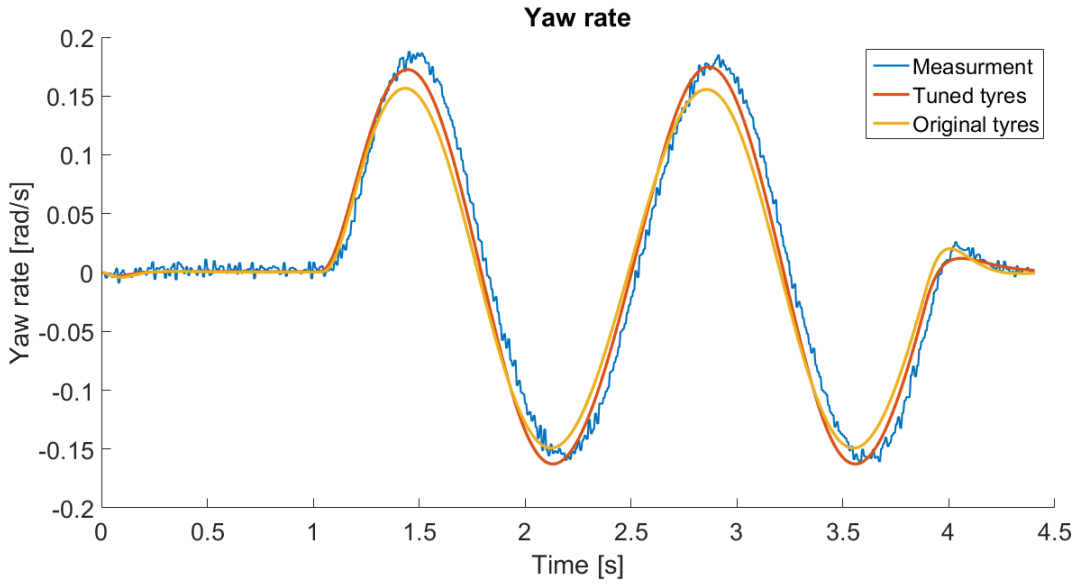

Figure 4.12: Comparison between tuned tyres,original tyres and measurements in yaw rate for an On Centre manoeuvre with a frequency of 0.7 Hz

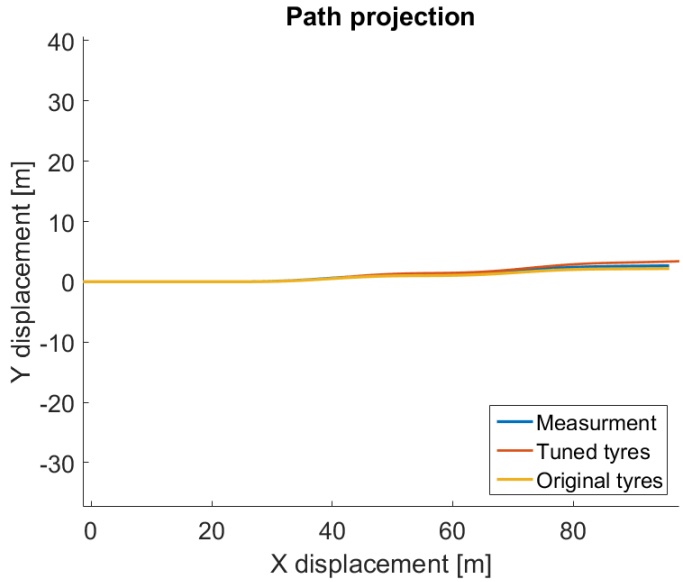

Figure 4.13: Comparison between tuned tyres,original tyres and measurements in path projection for an On Centre manoeuvre with a frequency of 0.7 Hz

The Measurement Based Method derived the aligning torque parameters with the use of measured tie-rod forces. Rack force was derived from the tie-rod forces and the aligning torque parameters were tuned until the rack force received from the CRT-model was the same as the derived rack force from the DNA data. However when the aligning torque parameters where tuned so the same rack force was achieved in the measurements as well as in the CRT-model it was found that for other manoeuvres oscillations of the rack force occurred. To ensure that the CRT-model would be stable when running in the driving simulator it was decided that the aligning torque parameters would not be tuned and instead be kept to remain stability. The difference in rack forces for a Constant Radius manoeuvre between the measurement and the tyre without tuned aligning torque parameters can be seen in

figure 4.14.

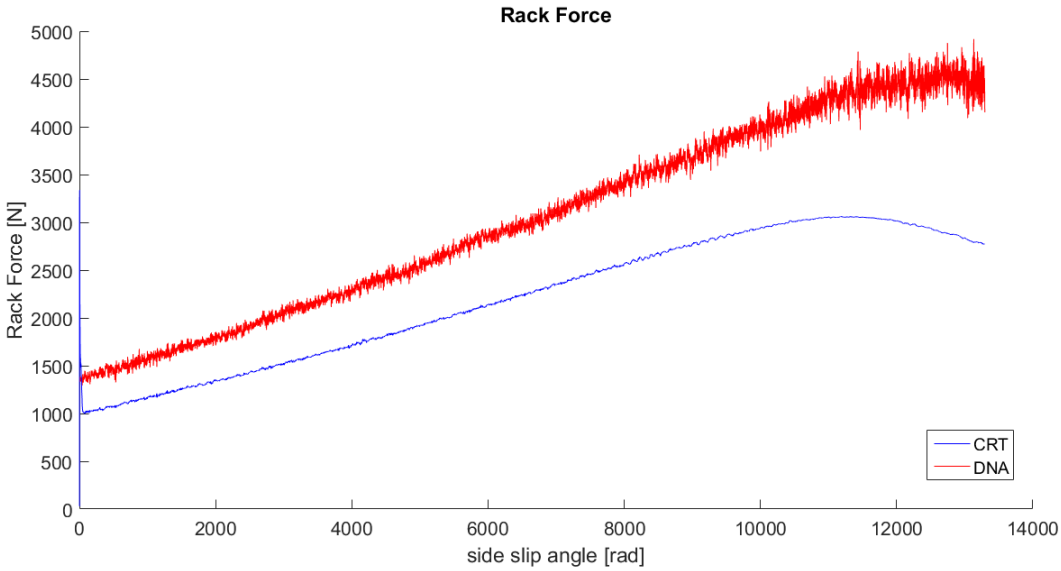

Figure 4.14: Rack force correlation between measurements and CRT for the Measurement Based Method

The Estimation Based Method used a physical tyre model to link together the lateral characteristics to the aligning torque. Due to that the CRT-model uses a tyre data sheet based on the Magic Tyre Formula the brush model had to be fitted to the Magic Tyre Formula parameters. Therefore was several side slip angle sweeps ran with different normal loads, even steps between 2000 N - 8000 N, for the Brush Model to increase the number of operation points and allow for a more valid fit. The result can be seen in figure 4.15. One can see that the curves differs from each other and a good fit could not be achieved which shows the difference between the Brush Model and the Magic Tyre Formula and which limitations are introduced when using a Brush Model.

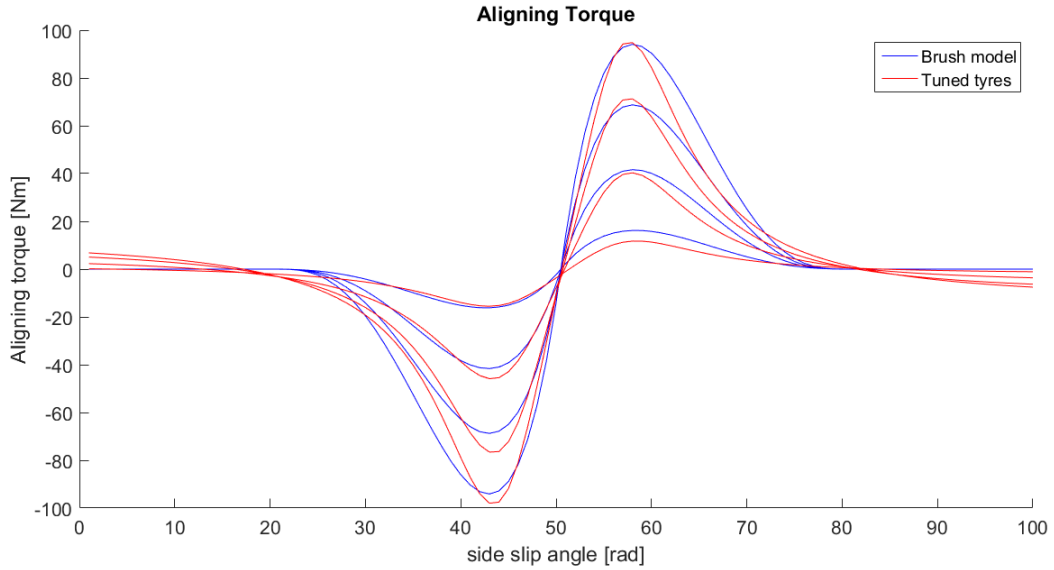

Figure 4.15: Aligning torque correlation between Brush Model and tuned tyre for the Estimation Based Method

4.3 Steering model

In this section the results from three different setups is presented. Two setups is created from the Measurement Based Method, one where the steering system is studied independently and one where the full model is used. A setup based on the Estimation Based Method is also created.

4.3.1 Measurement Based Method, Independently

This setup evaluates the steering system independently from the vehicle model and is purely based on measured values. No simulations in CRT are needed. The purpose of this setup is to visualise how the steering system is performing without a simulated vehicle model and by that evaluates how well the steering parametrisation performs in case of an ideal vehicle model. The base torque table is presented in figure 4.16. The friction and damping parameters used for both setups in the Measurement Based Method are presented in table 4.1.

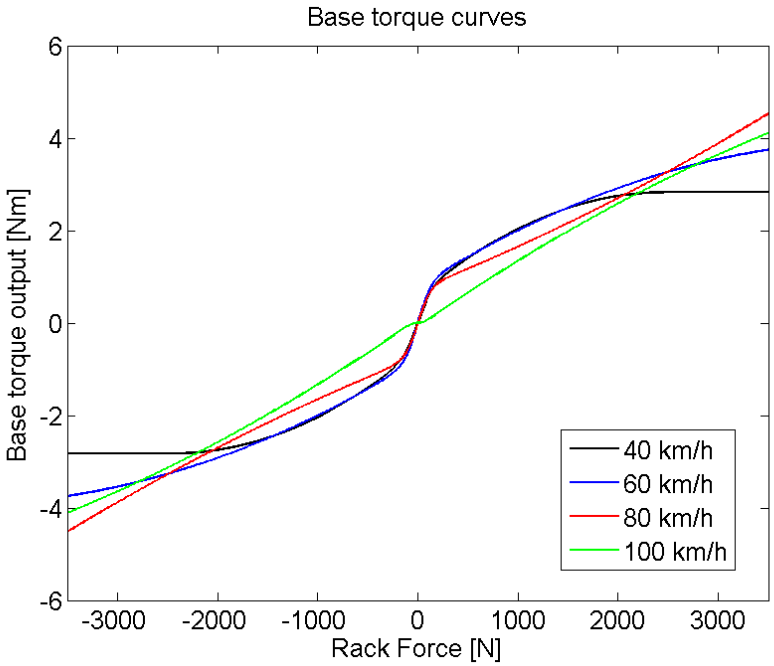

Figure 4.16: Base torque table created with measured rack forces following the Measurement Based Method

Table 4.1: Friction and damping parameters for the Measurement Based Method

Parameter	**Value**	**Unit**
C_max	0.4	Nm/(rad/s)
C_min	0.2	Nm/(rad/s)
κ	1.2	-
Friction	0.35	Nm

In figure 4.17 the results from the measured versus simulated HSS manoeuvre for 80 km/h is presented. The plot indicates a good correlation in terms of both shape and amplitude. The peak in the beginning in the measurements, at approximately 1.1 seconds is probably an measuring error in the steering robot.

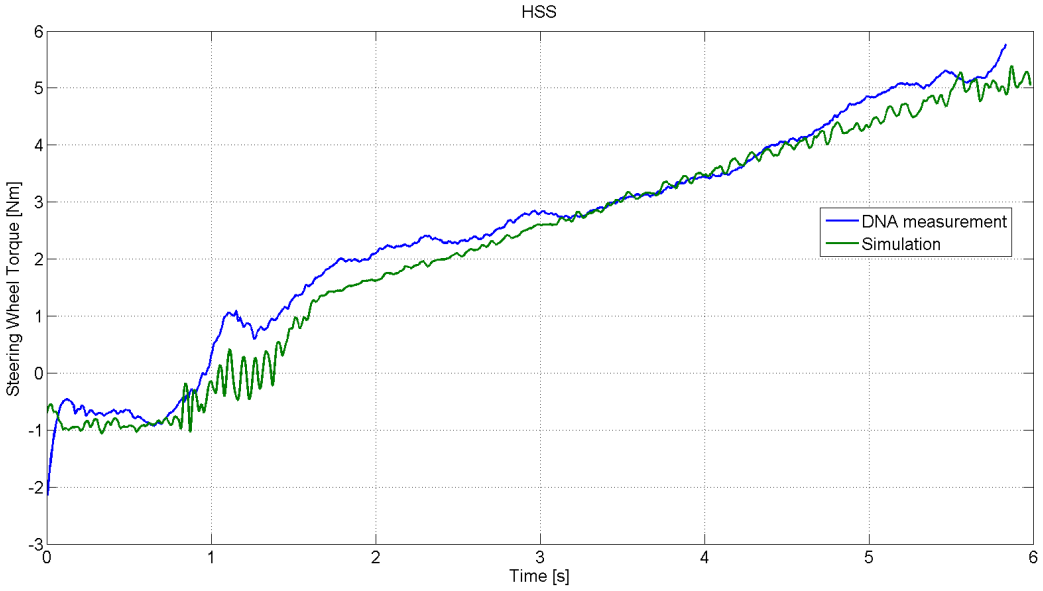

Figure 4.17: Correlation between independently steering system and DNA measurements for steering wheel torque vs time for a HSS manoeuvre at 80 km/h

The figures 4.18 and 4.19 presents the correlation of steering wheel torque between simulated and measured values for an On Centre manoeuvre performed in 40 km/h, 0.2 Hz and a maximum measured lateral acceleration of 0.2 m/s^2. The plot indicates a small underestimation of the simulated torque. The steering wheel velocity is low for a steering frequency of 0.2 Hz which result in low damping torques.

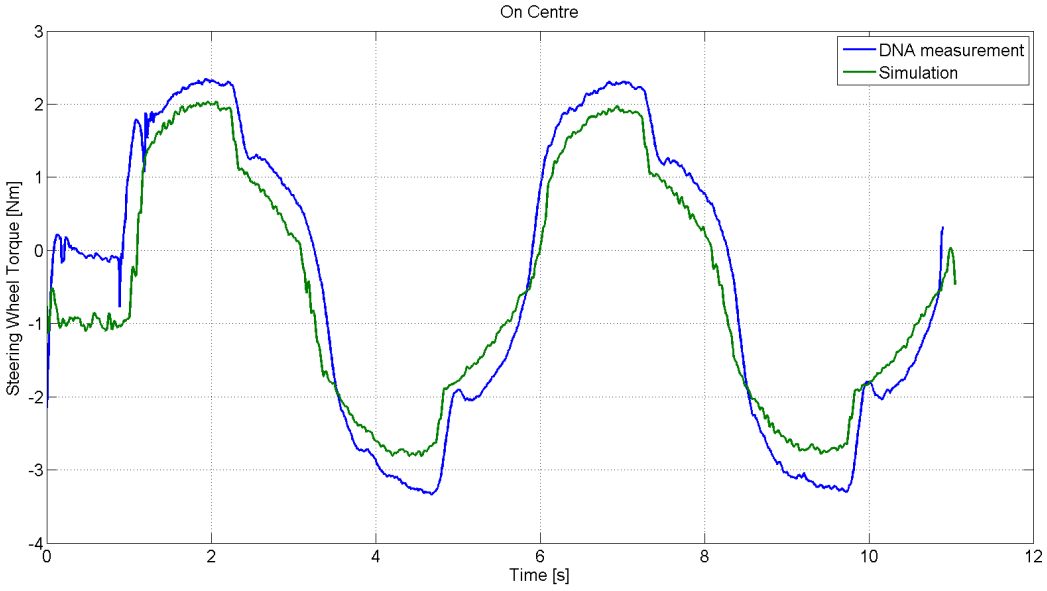

Figure 4.18: Correlation between independently steering system and DNA measurements for steering wheel torque vs time for an OC manoeuvre at 40 km/h and 0.2 Hz

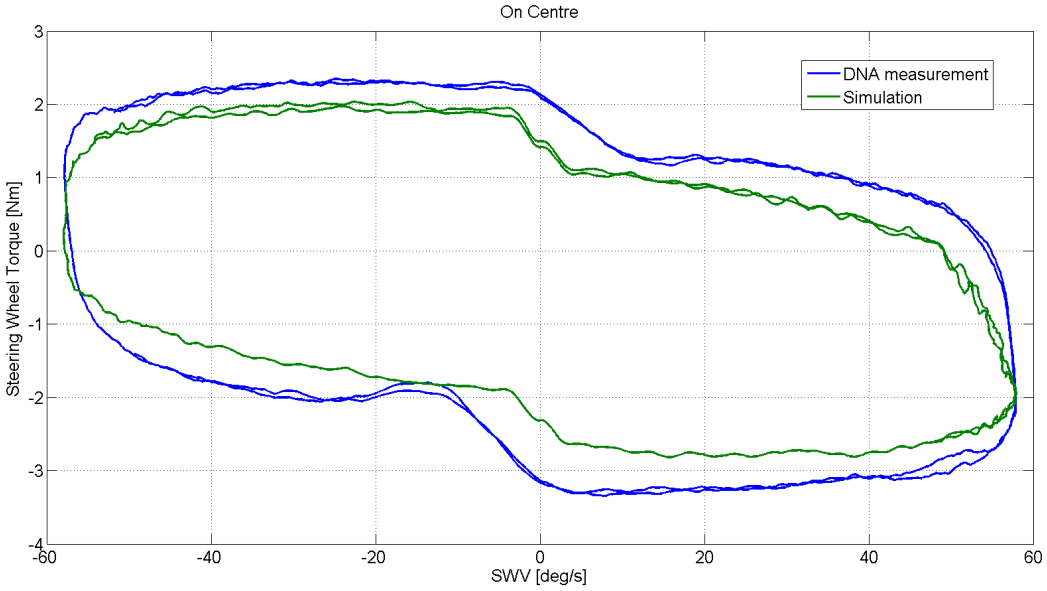

Figure 4.19: Correlation between independently steering system and DNA measurements for steering wheel torque vs steering wheel velocity for an OC manoeuvre at 40 km/h and 0.2 Hz

The figures 4.20 and 4.21 presents the results for an On Centre manoeuvre at 80 km/h and with a steering frequency of 0.2 Hz. This is the manoeuvre for which the steering parameters were optimised. The optimised damping coefficient C_{Min} in equation 3.19 had to be lowered manually in order to get realistic results at higher frequencies, this gave a slightly less correlation at 0.2 Hz but an overall better behaviour. The shape of the curve matches the results well. One can can see a clear step down in the steering wheel torque when changing the sign of the steering wheel velocity at the peak torque. This hysteresis can mainly be derived from the direction of simulated friction in the steering system.

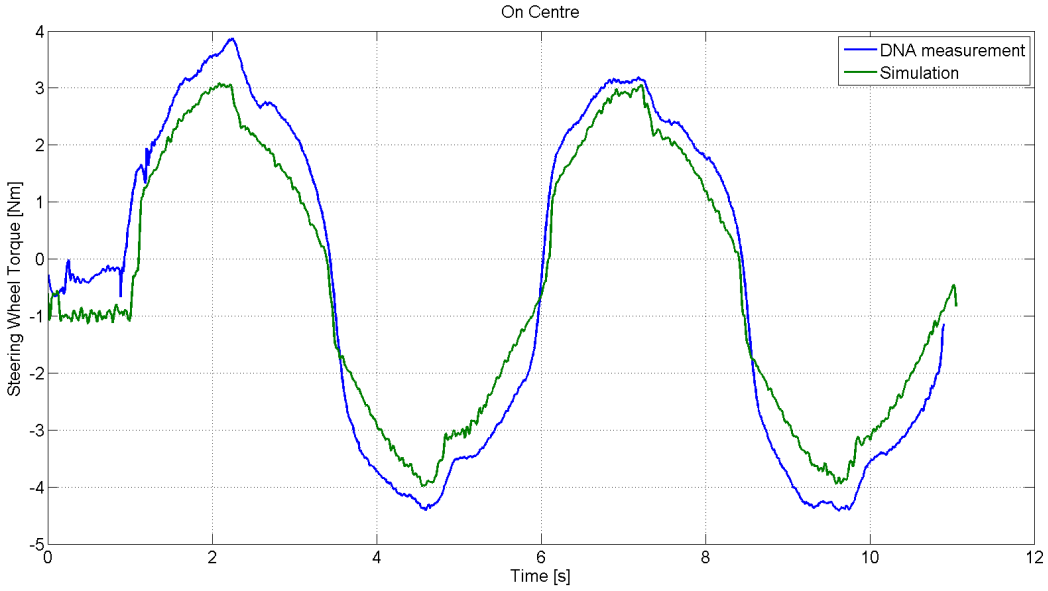

Figure 4.20: Correlation between independently steering system and DNA measurements for steering wheel torque vs time for an OC manoeuvre at 80 km/h and 0.2 Hz

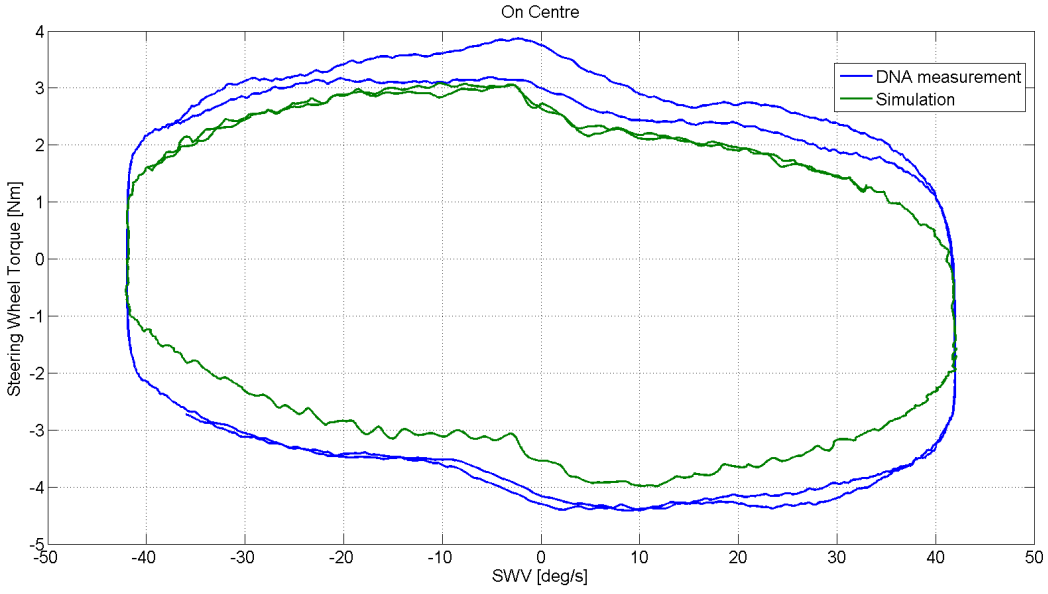

Figure 4.21: Correlation between independently steering system and DNA measurements for steering wheel torque vs steering wheel velocity for an OC manoeuvre at 80 km/h and 0.2 Hz

In figure 4.22 and 4.23 the result from the On Centre manoeuvre performed at the higher frequency of 0.7 Hz in 80 km/h is presented. The plots indicates an overestimated steering wheel torque output compared to the measuring data. The steering parameters were mainly tuned to give good results at lower frequencies, increasing the frequency more than three times, from 0.2 Hz to 0.7 Hz, resulted in

an overestimation. This could be because of shortcomings in the steering wheel velocity dependent algorithm in the steering system and active systems in the steering system of the test vehicle. It may also be derive from the steady state manoeuvre used when producing the base torque tables resulting in an underestimated assist torque from the steering system which would result in a higher torque output to the driver.

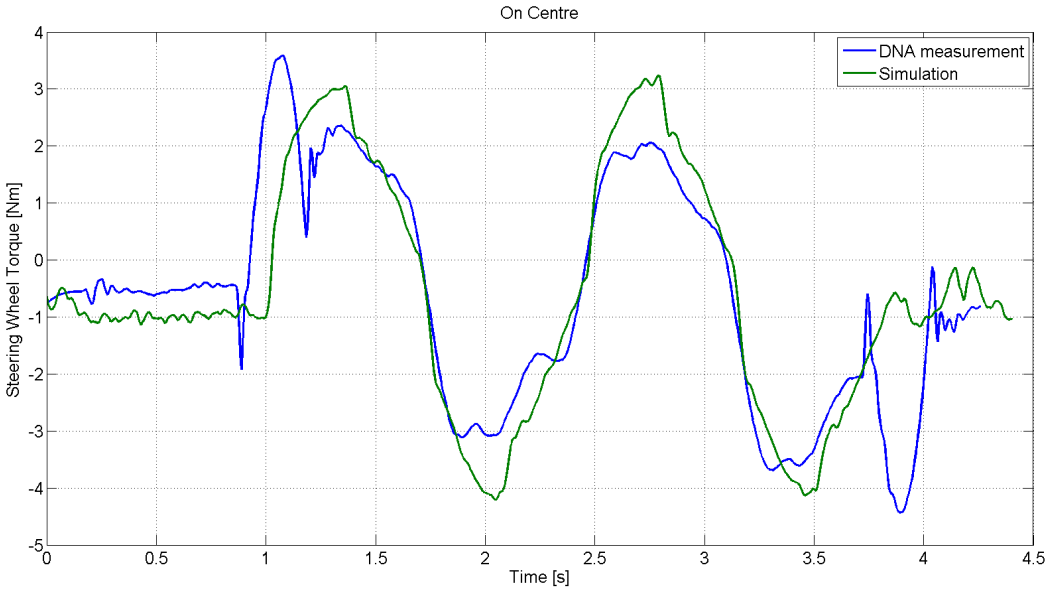

Figure 4.22: Correlation between independently steering system and DNA measurements for steering wheel torque vs time for an OC manoeuvre at 80 km/h and 0.7 Hz

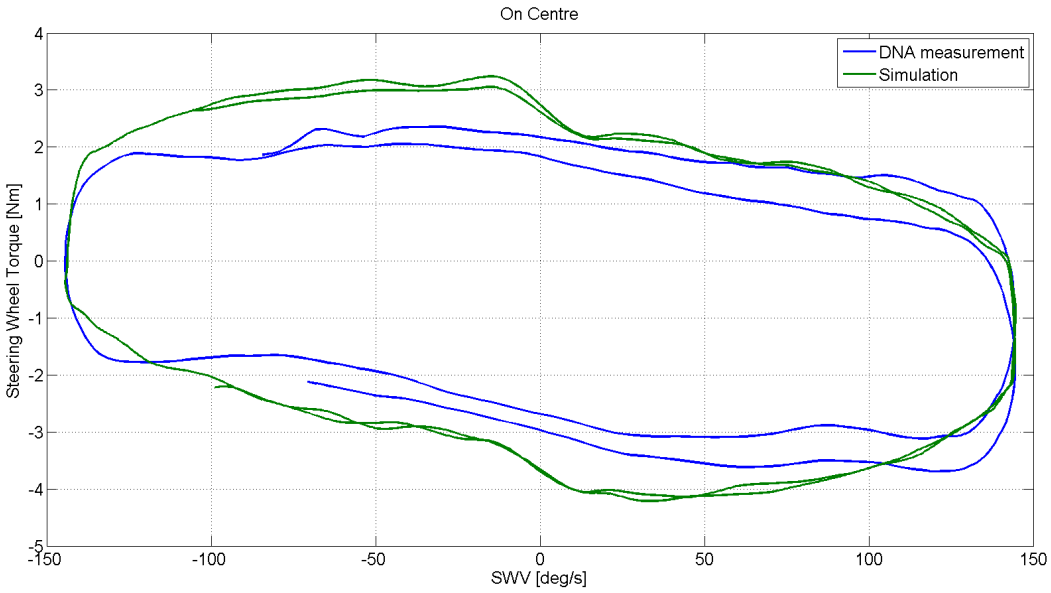

Figure 4.23: Correlation between independently steering system and DNA measurements for steering wheel torque vs steering wheel velocity for an OC manoeuvre at 80 km/h and 0.7Hz

4.3.2 Measurement Based Method, Simulator setup

The same base torque curves, figure 4.16, and parameters, table 4.1, as in the independent steering system setup are used in the simulator setup. This setup correspond for the actual Measurement Based Method used when running the model in the driving simulator. This model like the others are tested for HSS in 80 km/h and OC in 40 km/h with a frequency of 0.2 Hz as well as 80 km/h in both 0.2 Hz and 0.7 Hz. The simulator setup has an overall lower steering wheel torque output compared to the independent setup because of the underestimated simulated rack forces seen in figure 4.14. The results from the HSS manoeuvre in 80 km/h is presented in figure 4.24. The plot indicates a slightly underestimation of the simulated steering wheel torque which can be seen in all low transient manoeuvres with this setup.

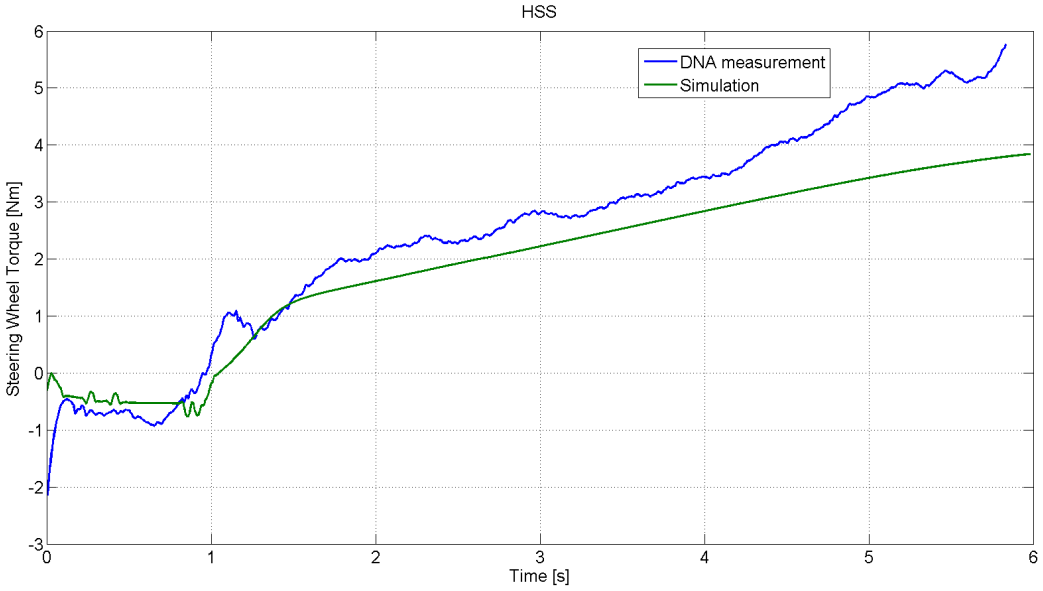

Figure 4.24: Correlation between Measurement Based Method and DNA measurements for steering wheel torque vs time for a HSS manoeuvre at 80 km/h

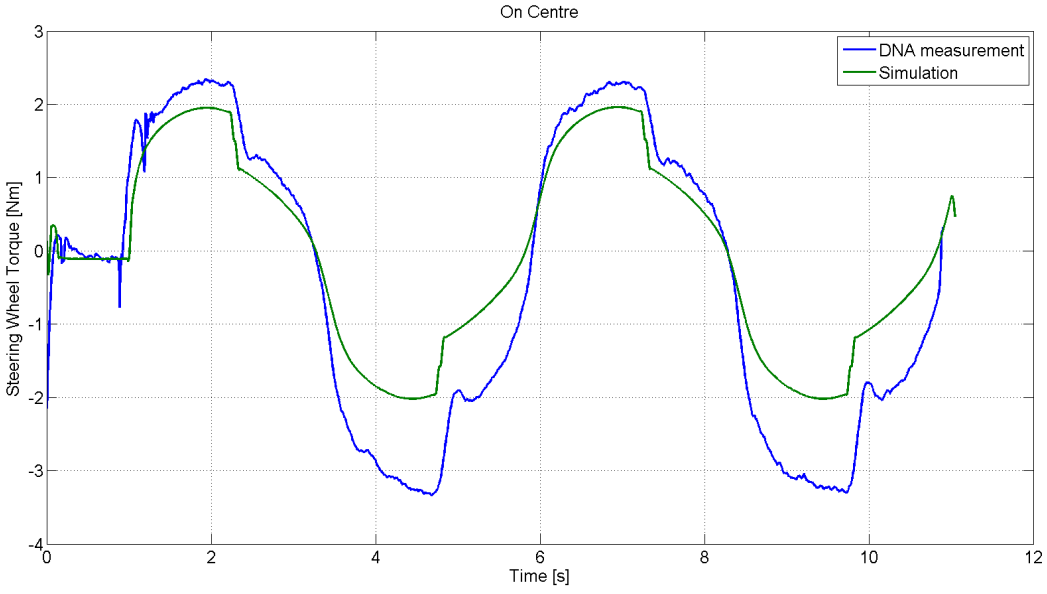

Figure 4.25: Correlation between Measurement Based Method and DNA measurements for steering wheel torque vs time for an OC manoeuvre at 40km/h and 0.2 Hz

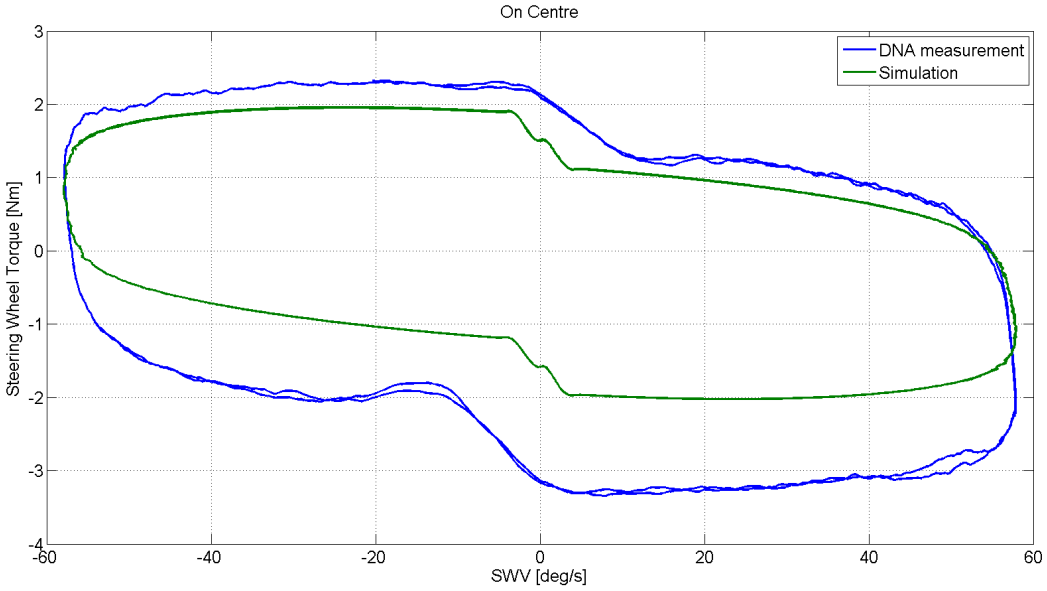

Figure 4.26: Correlation between Measurement Based Method and DNA measurements for steering wheel torque vs steering wheel velocity for an OC manoeuvre at 40 km/h and 0.2 Hz

Shown in figure 4.27 and 4.28 is the result from the On Centre manoeuvre at low frequency, 0.2 Hz, in 80 km/h. As mention earlier the steering wheel torque amplitude is underestimated in this simulation. The shape of the curve matches the measuring data well. Similar to the earlier results there is a clear hysteresis depending on the direction of the steering wheel velocity. The hysteresis indicates that it requires more torque from the driver to increase the steering angle than decreasing it which correlates well with the measurements.

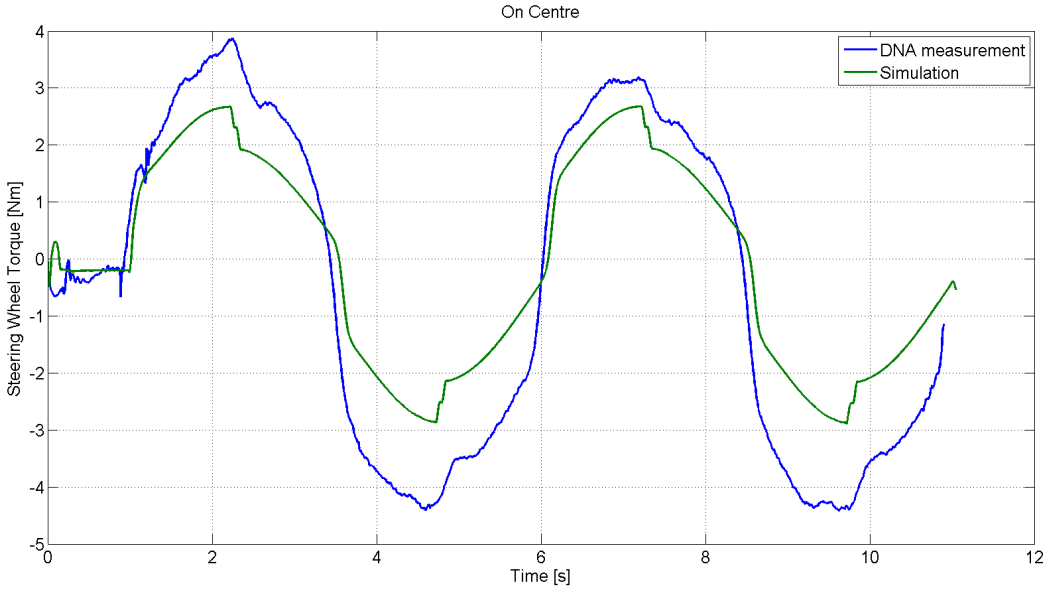

Figure 4.27: Correlation between Measurement Based Method and DNA measurements for steering wheel torque vs time for an OC manoeuvre at 80 km/h and 0.2 Hz

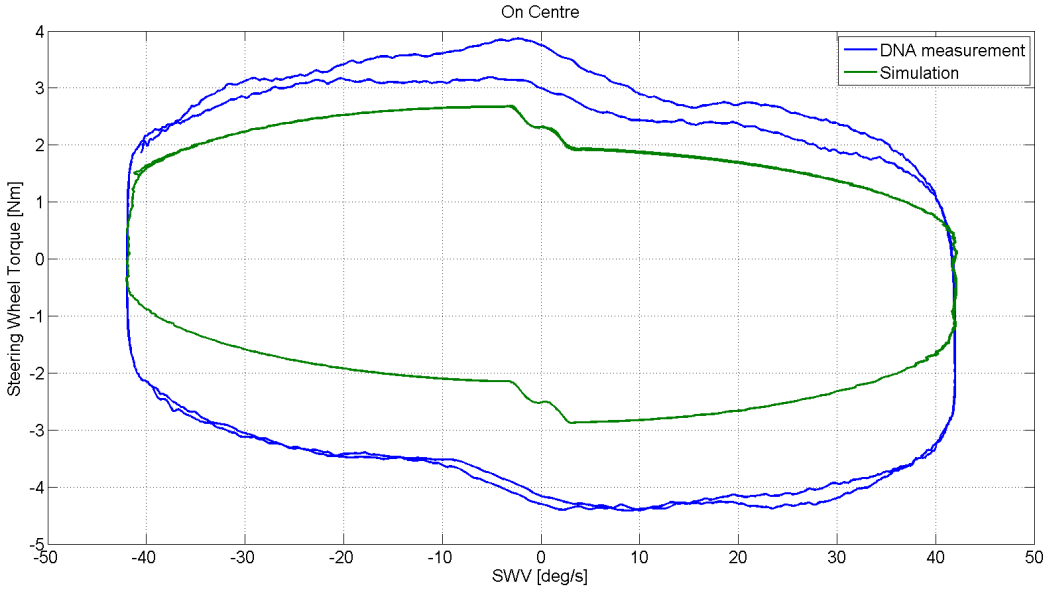

Figure 4.28: Correlation between Measurement Based Method and DNA measurements for steering wheel torque vs steering wheel velocity for an OC manoeuvre at 80 km/h and 0.2 Hz

The figures 4.29 and 4.30 presents the results from the high frequency On Centre manoeuvre of 0.7 Hz in 80 km/h. The plots show good correlation in terms of steering wheel torque amplitude for this manoeuvre. Earlier when studying the results from testing the independent steering system in figure 4.23 and 4.23 there was a clear overestimation of the steering wheel torque. In the simulator setup

the torque is underestimated for all the lower transient manoeuvres but results in a better match in terms of amplitude at this higher frequency. The measured data at the higher frequencies consist of more disturbances which makes it harder to do a good comparison of the shape of the curve.

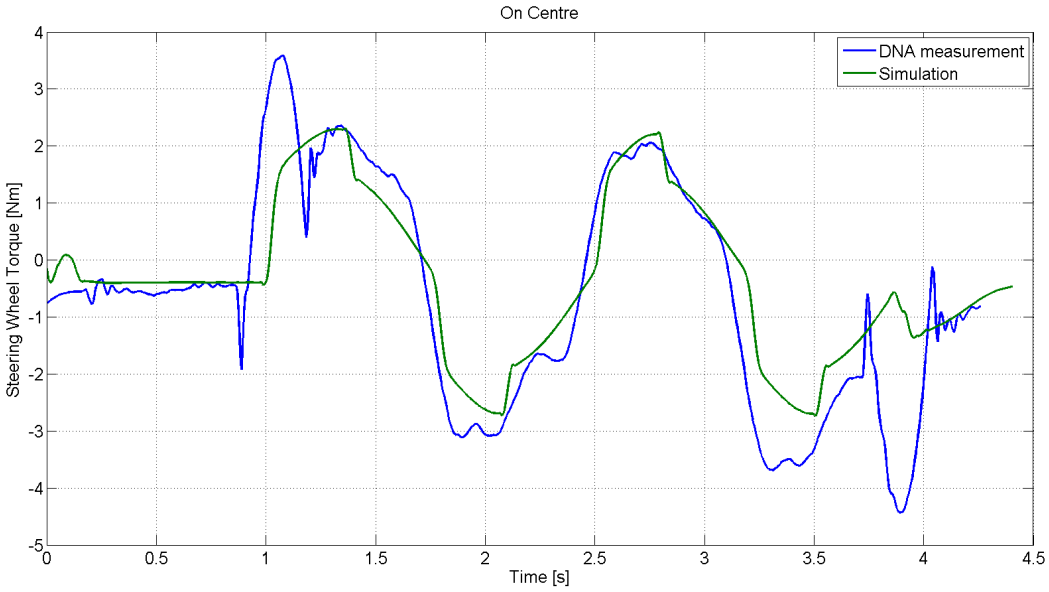

Figure 4.29: Correlation between Measurement Based Method and DNA measurements for steering wheel torque vs time for an OC manoeuvre at 80 km/h and 0.7 Hz

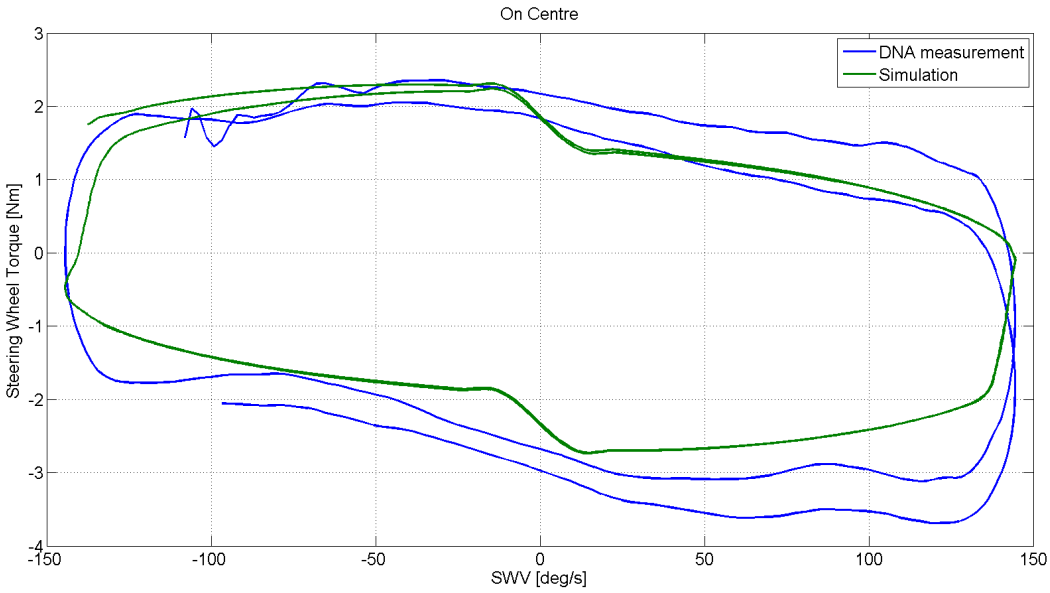

Figure 4.30: Correlation between Measurement Based Method and DNA measurements for steering wheel torque vs steering wheel velocity for an OC manoeuvre at 80 km/h and 0.7 Hz

4.3.3 Estimation Based Method

In this section the results from the steering system created with the Estimation Based Method is presented. The base torque table created from HSS data is depicted in figure 4.31. The parameters used in this method are defined in table 4.2. The parameters were optimised for an On Centre manoeuvre in 80 km/h with a frequency of 0.2 Hz where the lateral acceleration from the corresponding DNA-data reached 0.4 g. The lowest damping coefficient had to be lowered manually also for the Estimation Based Method.

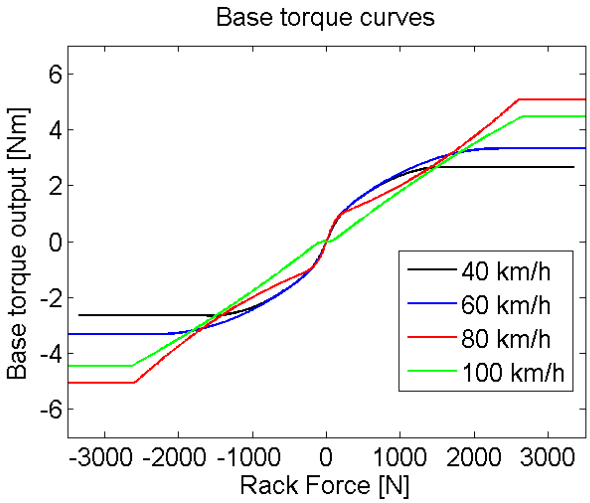

Figure 4.31: Base torque table from simulated rack forces using Estimation Based Method

Table 4.2: Friction and damping parameters for the Estimation Based Method

Parameter	**Value**	**Unit**
C_max	0.8	Nm/(rad/s)
C_min	0.5	Nm/(rad/s)
κ	1.4	-
Friction	0.35	Nm

The HSS manoeuvre performed in 80 km/h is represented by figure 4.32. This is the manoeuvre used when producing the base torque table and does thereby give an over all good correlation. One can see that at the end of the manoeuvre the simulated steering wheel torque exceeds the base torque tables validation region since it achieves a constant torque.

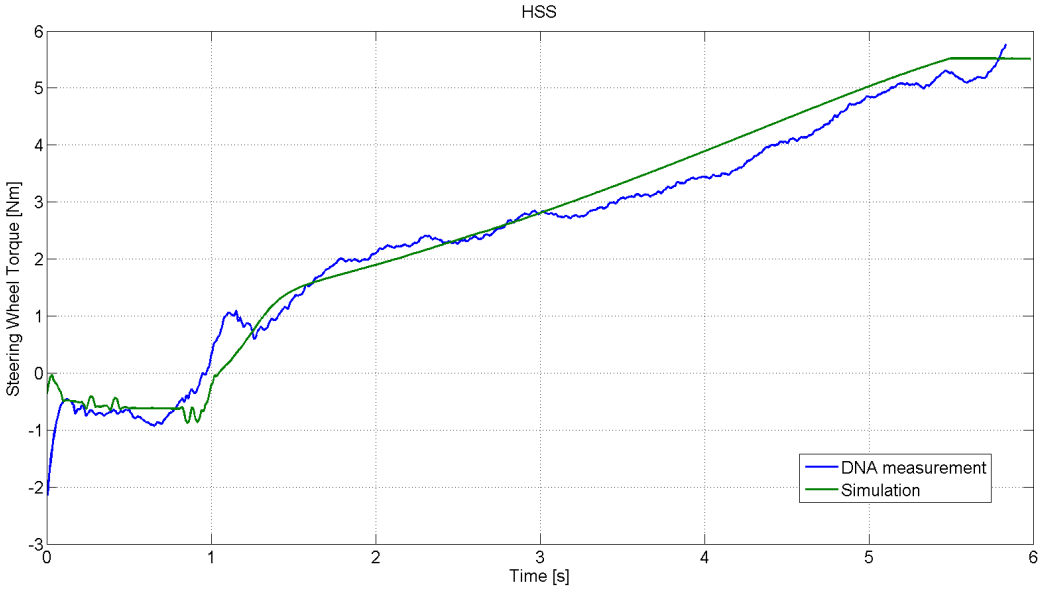

Figure 4.32: Correlation between Estimation Based Method and DNA measurements for steering wheel torque vs time for a HSS manoeuvre at 80 km/h

The result in figure 4.33 and 4.34 represent an On Centre manoeuvre in 40 km/h with a steering frequency of 0.2 Hz. The result indicates a slight underestimation of the amplitude but a good overall shape in the torque versus time plot. The steering wheel torque versus steering wheel velocity indicates an underestimation of the steering wheel torque for all velocities.

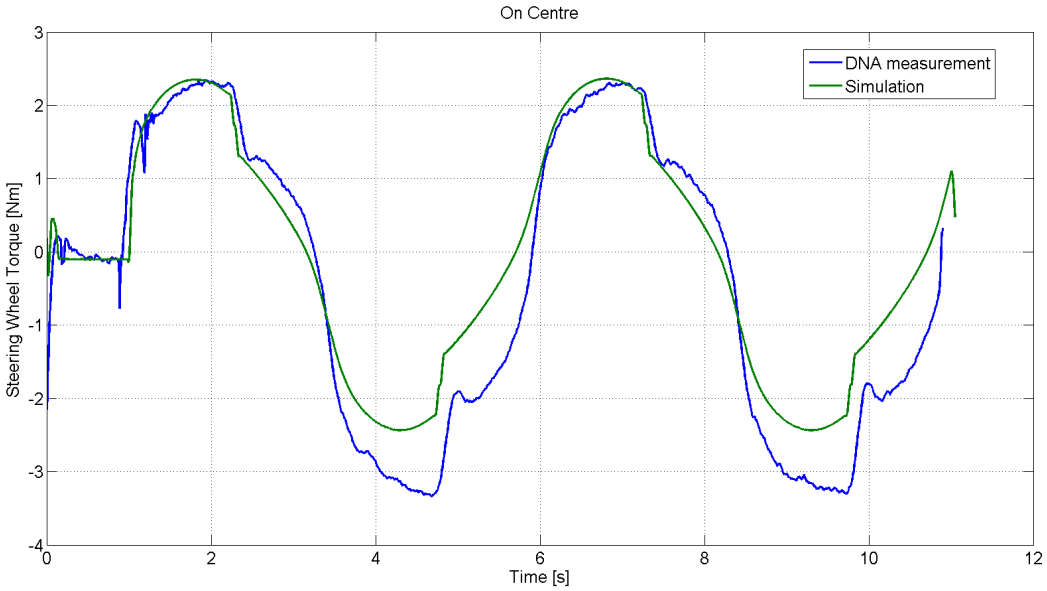

Figure 4.33: Correlation between Estimation Based Method and DNA measurements for steering wheel torque vs time for an OC manoeuvre at 40 km/h and 0.2 Hz

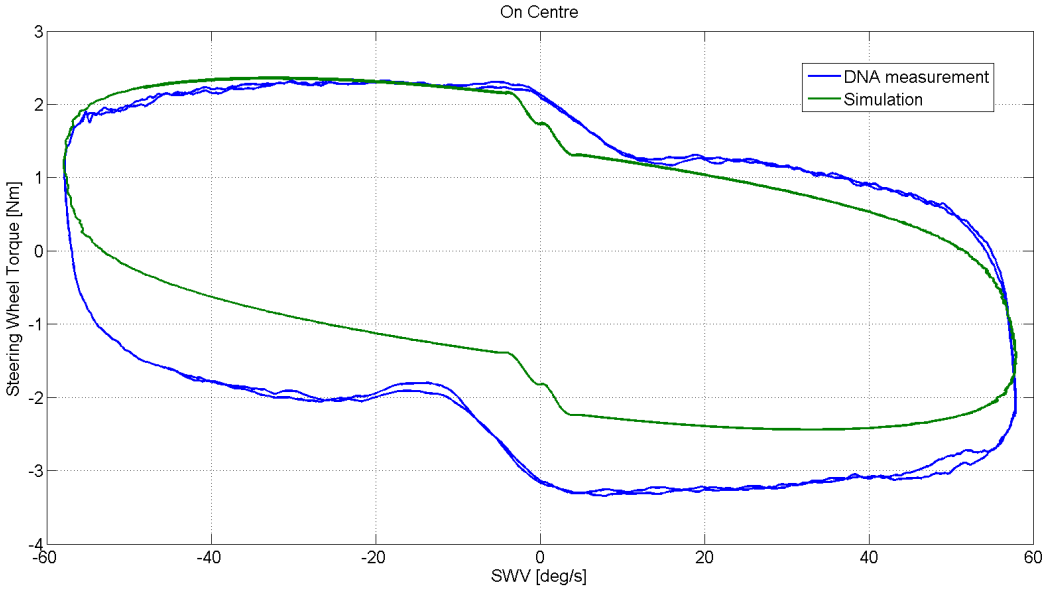

Figure 4.34: Correlation between Estimation Based Method and DNA measurements for steering wheel torque vs steering wheel velocity for an OC manoeuvre at 40 km/h and 0.2 Hz

In figure 4.36 and 4.35 the results from the On Centre manoeuvre in 80 km/h and 0.2 Hz is presented. The result indicates good correlation in terms of both amplitude and shape. Studying the shape of the steering wheel torque versus steering wheel velocity diagram one finds that the correlation is worse at high steering wheel velocities. This is probably an unwanted effect of the manual lowering of the damping in order to get a better match even at higher steering frequencies.

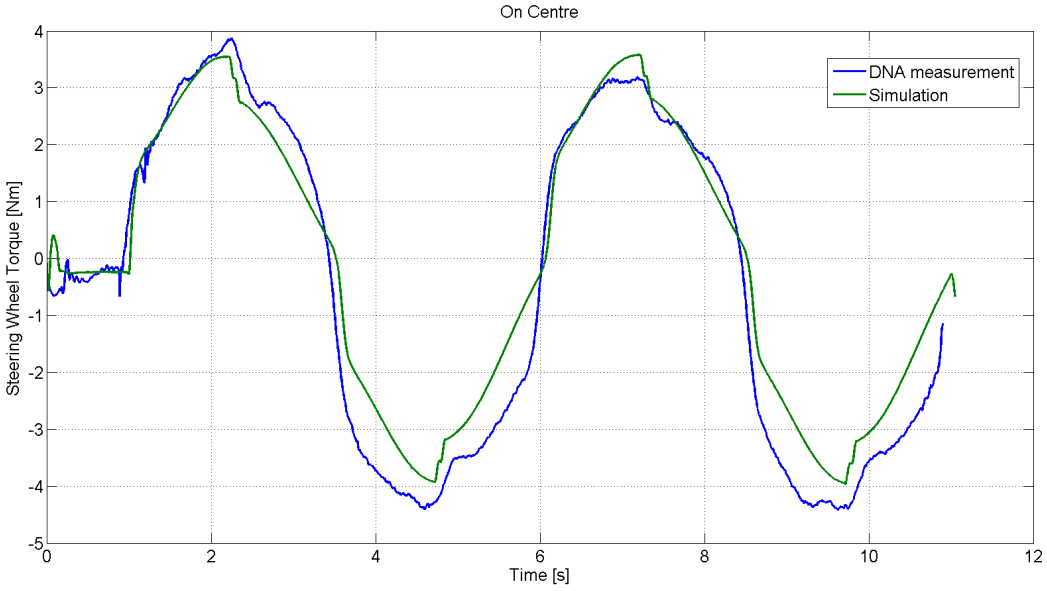

Figure 4.35: Correlation between Estimation Based Method and DNA measurements for steering wheel torque vs time for an OC manoeuvre at 80 km/h and 0.2 Hz

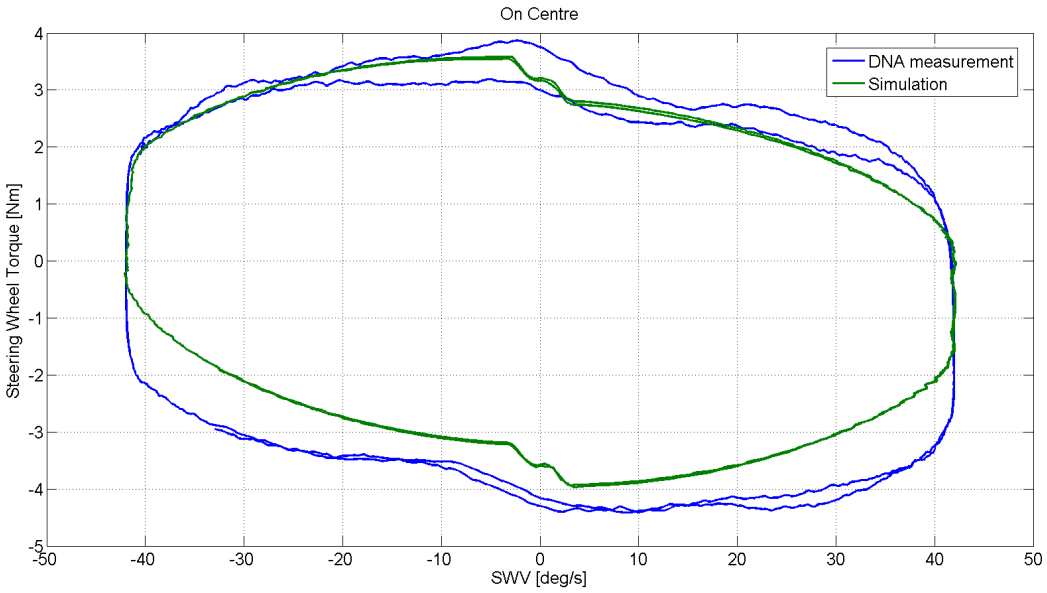

Figure 4.36: Correlation between Estimation Based Method and DNA measurements for steering wheel torque vs steering wheel velocity for an OC manoeuvre at 80 km/h and 0.2 Hz

The figures 4.37 and 4.38 represents the result from the On centre manoeuvre in 80Km/h with an relatively high frequency of 0.7 Hz. The plots from this test indicates an overestimated steering wheel torque amplitude similar as the results noted in Measurement Based Method for independently steering system, 4.22. As mention earlier the measurement data consist of more disturbance at higher frequencies which makes it harder to analyse the shape of the curve, especially in the steering wheel torque versus steering wheel velocity diagram in figure 4.38.

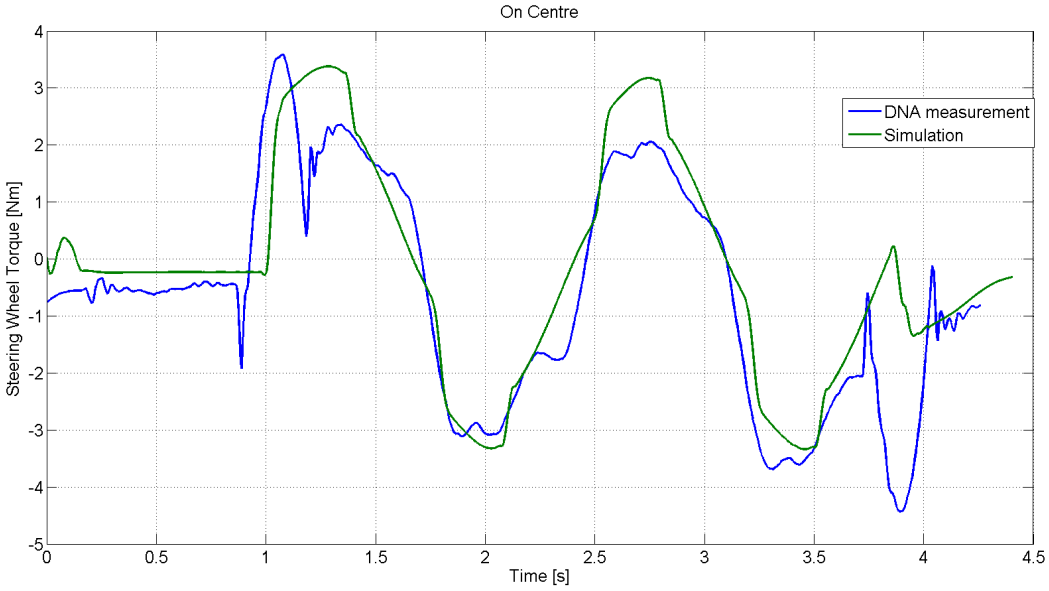

Figure 4.37: Correlation between Estimation Based Method and DNA measurements for steering wheel torque vs time for an OC manoeuvre at 80 km/h and 0.7 Hz

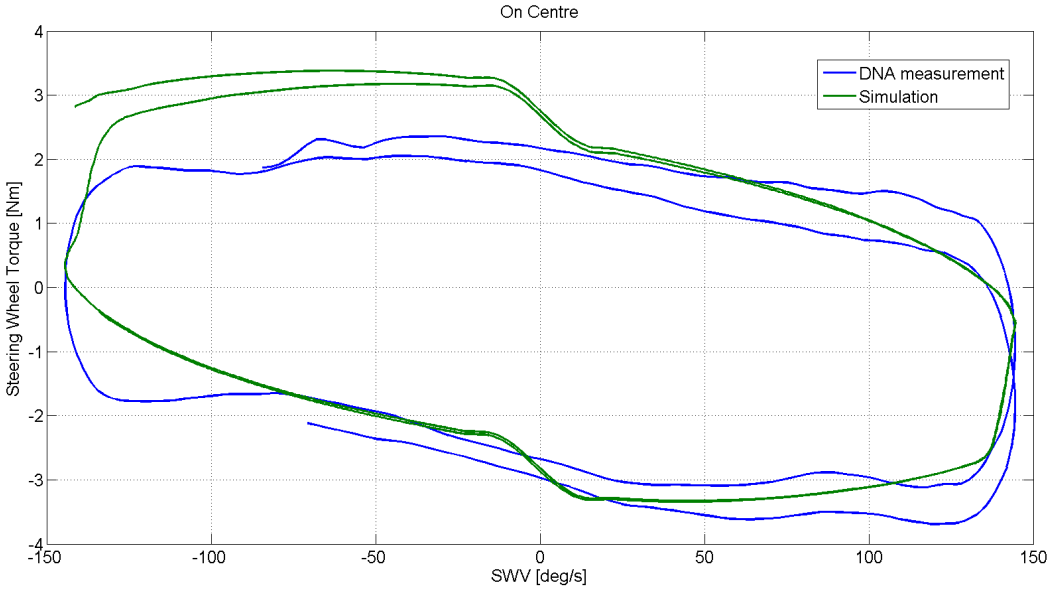

Figure 4.38: Correlation between Estimation Based Method and DNA measurements for steering wheel torque vs steering wheel velocity for an OC manoeuvre at 80 km/h and 0.7 Hz

4.3.4 Subjective Evaluation In Driving Simulator

Subjective evaluation was performed by inviting test drivers to run the different models in the driving simulator. They filled in a form regarding handling and steering with where they rated the model according to different criteria. This was a part of the development process. There was no evaluation

performed of the final models presented in this thesis but the models where tested. According to the drivers both the Measurement Based Method and the Estimation Based Method gave a well working torque feedback for On Centre driving in vehicle velocities between 40 - 80km/h. The steering wheel torque feedback was lower at higher velocities which it should according to the measurements from the HSS manoeuvres used when creating the base torque tables. However, a lower steering wheel torque at higher velocities is not wanted and when driving the vehicle on the test track the decreasing steering wheel torque at higher velocities was not noted. The tests performed at the highest velocity should therefore be studied to see if the correct measurements are received. An issue found was that the range of the base torque table was limited. When the rack force exceeds the maximum measured value in the table the steering wheel torque feedback become constant. However both models showed to be stable. The Measurement Based Method had underestimated the steering rack force which led to lower torque feedback and was perceived as giving a light steering feel. The method was however thought to give an overall better feedback and was therefore rated higher than the Estimation Based Method.

5 Discussion

This chapter contains discussion about the outcome of this thesis. The vehicle, tyre and steering model as well as the quality of measurement data are treated.

5.1 Vehicle Model

The tyre tuning concept is based around that the compliance and ratio between the steering wheel and the wheel can be derived from K&C tests with high accuracy. In this thesis the torque sweep test on the K&C-rig which was thought to receive the steering compliance gave poor result which has been explained earlier in section 4.1. The steering compliance was instead manually tuned during this thesis. A similar test but with the tyre swapped out with rigid replacements could result in a higher accuracy when determining the steering column compliance. A delimitation of the developed method is that it shall not require more than two extra days of measure and no changes are allowed to the vehicle which is not resettable. The method used in this thesis fulfils these but the Measurement Based Method requires that spare tie rods are ordered in advance.

Three levels of instrumentation on the test vehicle was planned in this thesis. The equipment for reference level was not available during the thesis which resulted in the reference level was not carried out. The data from the reference level would had resulted in a higher grade of validation of the vehicle models. The optical wheel angle measurement system would have given data to validate the simulated slip and camber angles during the measurements. The measuring wheels would have given the forces during the manoeuvres which could be used to evaluate the tyre characteristics.

5.2 Tyre Model

The Genetic Algorithm that was used requires a high number of iterations and a large population to minimise the error. With the need of running a CRT simulation within every proposed solution it became a very time consuming process. Due to time limitations the tyre data optimisation was limited in number of iterations the optimisation could run which could result in that the parameters receive is not necessary the optimum solution.

The Constant Radius manoeuvre that was used as the tuning manoeuvre could be improved by starting at 30 km/h which would allow the CRT-model to start in the same state as the DNA data. To be able to capture more of the saturation peak in lateral acceleration it would be beneficial to run the test longer and include some off-tracking to get more of the saturation peak. As the manoeuvre is designed today the vehicle will follow a Constant Radius and an off-tracking due to saturation would result in that the steering wheel robot would apply maximum steering wheel angle to try to compensate the error. If the steering wheel angle would be inserted as the steering input in the CRT-model the tyre would be forced to saturate due to the increase in steering wheel input even if the tyre could achieve a higher peak force. This could result in that the peak factor would not be able to be determined accurately. An alternative steering input would be that at high longitudinal velocities the steering wheel angle would become constant to avoid a rapid increase in steering wheel angle at tyre saturation. Another alternative would be to lower the rate of change the robot can adjust the steering wheel angle and by that have a slower increase in steering wheel angle at tyre saturation.

It was first decided that the tyres would be tuned against two different normal load setups in a Constant Radius manoeuvre, one with the load curb+2 and one with maximum load. This was thought to receive a higher accuracy of the normal load dependency in the tyre variables. When received the result from the DNA measurements it showed that only two runs, one in each direction, was able to be ran within the time limit that was set for the DNA testing for the setup with maximum load. It was also seen that the test was started at slightly different velocities. This resulted in a high

uncertainty for the setup with maximum load which resulted in that the maximum load was not considered and instead only the curb+2 setup was studied.

The way the relaxation length was derived was by using an approximation. Another way to derive the relaxation length could be to tune the relaxation length parameters against an On Centre manoeuvre which could result in a higher accuracy. However when tuning for an On Centre manoeuvre the whole CRT-model would be used which could result in that more then the tyre characteristics can influence the result. This is however nothing that has been investigated further in this thesis.

When tuning the aligning torque parameters using the Measurement Based Method oscillations were received. This resulted in that the parameters were not tuned and instead was kept so the CRT-model remained stable and could be ran in the driving simulator. The reason that some combinations of the aligning torque parameters creates oscillations needs to be investigated further before being able to tune the aligning torque parameters according to the Measurement Based Method.

The thought around the Estimation Based Method was that errors induced in the aligning torque characteristics due to the use of a Brush Model could be compensated for in the base torque curves. For instance could an overestimated aligning torque be compensated for by that the base torque curves would be lower. However the shape of the aligning torque and the normal load dependency can not be compensated by the base torque curve. The Brush Model is a simple physical tyre model which was chosen due to it requires little information about the tyres and could therefore be determined with the information provided. However the drawback with the Brush Model is that it has low information about the tyres and therefore can the resulting aligning torque calculated deviate from the actual aligning torque. This results in that the Estimation Based Method has a high uncertainty factor when it comes to subjective correlation even though the objective comparisons show good correlation.

5.3 Steering Algorithm

The inertial effects in the steering system was not modelled due to noise problems when calculating the time derivative of the steering wheel velocity. The friction and damping showed to have a very limited tuning possibilities. When increasing the damping at low steering wheel velocities as well as friction in order to get a higher steering wheel torque output one also lowers the base torque table. This due to the method used when creating it by subtracting the estimated damping and friction for the used HSS manoeuvre. The damping and friction parameters used are constant relative to the vehicle velocity. A future improvement could be to investigate if these parameters are vehicle velocity dependant and that the dependency correlates to additional functions in the steering system. Studying the results one can see that the simulated steering torque matches best for the manoeuvres where the parameters have been optimised. There is a clear similarity between the two base torque plots in 4.16 and 4.31. The velocity dependency is smaller than expected but one can see that the shape varies between the velocity steps. The base torque curves have only been fitted for the range of measurement values and with the torque being saturated for inputs outside the measured region. The base torque table was shown to be limited. This could probably be improved by implementing a function that calculates how the curve is supposed to continue. One solution could be to calculate the inclination of the curve for the last measurement values and keep that inclination for the resulting rack forces. Some of the quadratic equations used in the current curve fit method had a positive shape that would result in too high steering wheel torque if continuing with the same equation at higher rack forces. An improvement of the base torque creation would be to take the mean value of multiple test of the same manoeuvre. This would probably reduce test specific disturbances and give higher fidelity to the measurements.

The result from the HSS manoeuvres at 80 km/h for the Measurement Based Method with independently steering system and the Estimation Based Method indicates both on good correlation with the measurement data. But the results from the Measurement Based Method with the simulator

setup indicates an underestimation of the steering wheel torque. This is most probably due to the underestimation of the rack forces as already mentioned. By running a parameter optimisation for the simulator setup instead of using the same parameters for both Measurement Based Method setups could probably improve the results. However, the simulator setup of the Measurement Based Method indicates good correlation at the higher frequency of 0.7 Hz seen in figure 4.29. The same manoeuvre is otherwise overestimated in both the independent steering system setup of the Measurement Based Method as well as in the Estimation Based Method, figure 4.22 and 4.37. The reason for the overestimation is that the damping parameters are mainly optimised for lower frequencies. Preferably the model would have been optimised for a wider range of manoeuvres. The deviation can also come from the influence of active functions in the steering system and could require for instance vehicle velocity dependent parameters.

Even if the rack force is underestimated the steering wheel torque output correlates well for the Estimation Based Method. This is because the base torque table has created a relation between the underestimated force and steering wheel torque. The table will thereby deliver a well matching base torque when running the final vehicle model even if the the rack force is underestimated. The black box modelling used in the Estimation Based Method focusing on delivering the correct final torque output even if specific components within the system delivers incorrect values. According to the subjective test sessions the Measurement Based Model had a lower steering wheel torque than the Estimation Based Model. This corresponds well with the objective data achieved by the simulations. The test driver tended to grade the simulator setup of the Measurement Based Method higher when it comes to steering feedback even if the objective results shows a slightly better correlation for the Estimation Based Method. The overall results from the steering models shows better correlation at manoeuvres with lower frequencies.

5.3.1 Quality of Data

The overall data received from the measurements had low noise levels and the result from the number of runs for each manoeuvre showed reliability and reproducibility. The noise of the measured steering wheel torque seemed to increase with a higher steering frequency and required heavier filtering in order to be analysed. The increase in noise is probably because of errors in the measurement performed by the steering robot, it may be that the robot is affected by its own moment of inertia and includes this in the torque measured for high transient manoeuvres. The measurements received from the On Centre manoeuvre in 0.7 Hz contained high disturbances in the beginning and ending of the manoeuvre, as in figure 4.22. This could indicate that in the beginning and ending of the manoeuvre the controller of the steering robot induces disturbances. Studying the data achieved from the HSS manoeuvre in 80 km/h as in figure 4.17 one can find the same torque peak in the beginning of the run. This is probably an error that derives from the rapid start of the steering robot manoeuvre.

6 Conclusion

The goal with this thesis was to develop a method of how a vehicle model of a competitor vehicle could be built from measurements and be driven in a driving simulator. Two methods has been presented in this thesis, one where the tie-rod forces was measured and one where a physical tyre model was used. By adding a few manoeuvres and equipment according to the method of interest a vehicle model could be built and tyres and steering system could be tuned to match the competitor vehicle characteristic. The methods requires high accuracy in steering compliance to achieve good tyre tuning. This is to minimise the error in the tyre parameters and increase the accuracy of both the steering system and the tyres on component level. The methods show good correlation against measured data for low transient manoeuvres although at higher transients the lateral acceleration and steering wheel torque was starting to differentiates against the measured data. Further refinement and validation of the methods needs to be done before being able to be used as established method methods. Both methods developed gives the same vehicle characteristics which means that objective measurements of vehicle behaviour performed in CRT will give the same results for the two methods. The difference between the methods is how the torque feedback is derived in the steering system. The difference will effect the objective and subjective evaluation of the steering system. The Estimation Based Method showed good correlations in the objective evaluation of the steering system. However, there is an uncertainty of how well the Brush Model capture the actual aligning torque and due to the poor correlation when tuning the parameters from Brush Model to Magic Tyre Formula the result has low accuracy. From what was noted during the subjective evaluation in the driving simulator the Estimated Based Method was rated lowest in torque feedback which indicates that the method does not give sufficient result. The Measurement Based Method showed lesser accuracy in objective measurements due to that the aligning torque parameters could not be tuned which resulted in underestimated rack force. In the subjective evaluation was the Measurement Based Method received with a higher rating which indicates on a higher resemblance to the actual steering system. The higher rating in subjective evaluation was thought to be that the aligning torque parameters was captured more accurate with the Measurement Based Method and was therefore seen as the more preferable method.

The valid range of the steering system was set by the range of the base torque table. The limited rack force range allows only for less aggressive manoeuvre such as HSS, OC, and CR to be performed without exceeding the valid region. The base torque table limits also the the lowest velocity to 40 km/h and the highest velocity to 100 km/h.

The presented methods makes it possible to extend the benchmarking process of competitor vehicles and allow the vehicle to be evaluated in additional environments such as the driving simulator and CRT. This allows the possibility to benchmark competitors vehicle in different stages during the development and increases the effectiveness of benchmarking as a tool.

7 Future Work

The developed method needs further work before it can be used as an established method for competitor vehicle benchmarking at Volvo Cars. Below are some of items that requires further work described.

- The vehicle model created in CRT deviates from the DNA data at high transient manoeuvres even with the tyre data for the tyres used during the DNA tests. This shows that the look-up table based model in CRT needs to be studied more to see if one can increase the accuracy for high transient manoeuvres. The rack force from the CRT-model was underestimated compared to measured measured data which increased the difficulty to tune the tyres and the steering system. Therefore needs further work to validate the CRT-model.
- The steering compliance was manually tuned in this thesis due to complications during the steering wheel torque sweep. Further work would be to study how to improve the test to receive higher accuracy when measuring the steering column compliance.
- Some combinations of the aligning torque parameters resulted in oscillations in the rack force. The cause for this needs to be investigated further before the Measurement Based Method could be used to tune the aligning torque parameters.
- In order to avoid reaching the constant limit when analysing steering wheel torque feedback in the driving simulator the range of the base torque table needs to be increased. The base torque table needs to be valid for higher vehicle velocities as well as for larger rack force.

References

[1] M. A. Acar and B. Ulaş. Benchmarking of Market Competitor Vehicles for Vehicle Dynamics Target Setting ().

[2] C. Andersson Eurenius and J. D. Cortiñas. Validation of a Moving Base Driving Simulator for Subjective Assessments of Steering and Handling (2015).

[3] *Calculations Reference Manual. Suspension Parameter Measuring Machine*. Anthony Best Dynamics Limited, 2013. URL: www.abd.uk.com.

[4] Engineers Edge, LLC. *Truck and Car Universal Joint Design and ENgineering Equation*. [Online: accessed June 20, 2016]. URL: www.engineersedge.com/power_transmission/universal-joint-design-calculations.htm.

[5] *EPS_Belt_Drive_2013-001*. [Online: accessed June 10, 2016]. 2013. URL: cnet2.cbsistatic.com/hub/i/r/2014/02/11/78aa3556-a5e1-11e3-a24e-d4ae52e62bcc/resize/570xauto/e911653687ff306a94693a900e176646/EPS_Belt_Drive_2013-001.jpg.

[6] S. Holmes. RMS Error (2000). URL: statweb.stanford.edu/~susan/courses/s60/split/node60.html.

[7] B. Jacobson. *Vehicle Dynamics Compendium for Course MMF062*. Preface 2015. Chalmers University of Technology ,Department of Applied Mechanics, Vehicle Engineering and Autonomous Systems, 2015.

[8] M. F. Kinstle, D. Hassler, and B. S. Johnson. *Vehicle dynamics benchmarking and simulation*. Tech. rep. SAE Technical Paper, 2009.

[9] J. S. Loeb et al. *Lateral stiffness, cornering stiffness and relaxation length of the pneumatic tire*. Tech. rep. SAE Technical Paper, 1990.

[10] H. Pacejka. *Tire and vehicle dynamics*. Elsevier, 2005.

[11] J. Reimpell and H. Stoll. *Automotive Chassis: Engineering Principles*. 1st. London: Arnold, 1996, pp. 247–282. ISBN: 1-56091-736-9.

[12] *Servolectric. Electromechanical steering system for a dynamic driving experience and highly automated functions*. BOSCH, 2015. URL: http://www.bosch-automotive-steering.com/fileadmin/downloads/Flyer_Nkw/AS_Systemmappe_Servolectric_E_lowres_20150513.pdf.

[13] *SPMM Controller. USER GUIDE*. Version 10.xx. Anthony Best Dynamics Limited, 2013. URL: www.abd.uk.com.

[14] The MathWorks, Inc. *How the Genetic Algorithm Works*. [Online: accessed June 12, 2016]. URL: se.mathworks.com/help/gads/how-the-genetic-algorithm-works.html.

[15] J. Y. Wong. *Theory of ground vehicles*. John Wiley & Sons, 2001.

[16] Y. Xue and J. Watton. Modelling of a hydraulic power steering system. *International journal of vehicle design* **38**.2-3 (2005), 162–178.

8 Appendix

A Extended Magic Tyre Formula

Extending the Magic Tyre Formula, scaling factor are introduced which can be seen listed below. The scaling factors scales different tyre parameters due to the road condition, However in this thesis the scaling factors are set to 1.

Scaling factors (Pure slip)

λ_{Fz0} : Nominal (rated) load

$\lambda_{\mu x,y}$: Peak friction coefficient

$\lambda_{\mu V}$: With slip speed V_s decaying friction

$\lambda_{Kx\kappa}$: Brake slip stiffness

$\lambda_{Ky\alpha}$: Cornering stiffness

$\lambda_{Cx,y}$: Shape factor

$\lambda_{Ex,y}$: Curvature factor

$\lambda_{Hx,y}$: Horizontal shift

$\lambda_{Vx,y}$: Vertical shift

$\lambda_{Ky\gamma}$: Camber force stiffness

$\lambda_{Kz\gamma}$: Camber torque stiffness

λ_t : Pneumatic trail (effecting aligning torque stiffness)

λ_{Mr} : Residual torque

Reduction factors are also introduced in the extended Magic Tyre Formula which are set to 1 in this thesis.

$\xi_i = 1 \qquad i = 1, 2, 3, \ldots$

The factors in Magic Tyre Formula for lateral force at pure side slip can be extended to following expression:

$$F_{y0} = D_y \cdot \sin\Bigg(C_y \cdot \operatorname{atan}\Big(B_y \cdot \alpha_y - E_y(B_y \cdot \alpha_y - \operatorname{atan}(B_y \cdot \alpha))\Big)\Bigg) + S_{Vy} \tag{A.1a}$$

$$\alpha_y = \alpha^* + S_{Hy} \tag{A.1b}$$

$$C_y = P_{CY1} \cdot \lambda_{Cy} \quad (> 0) \tag{A.1c}$$

$$D_y = \mu_y \cdot F_z \cdot \xi_2 \tag{A.1d}$$

$$\mu_y = (P_{DY1} + P_{DY2} \cdot df_z) \cdot (1 - P_{DY3} \cdot \gamma^{*2}) \cdot \lambda^*_{\mu y} \quad (> 0) \tag{A.1e}$$

$$E_y = (P_{EY1} + P_{EY2} \cdot df_z) \cdot \Big(1 - (P_{EY3} + P_{EY4} \cdot \gamma^*) \cdot \operatorname{sign}(\alpha_y)\Big) \cdot \lambda_{Ey} \quad (\leq 1) \tag{A.1f}$$

$$K_{y\alpha 0} = P_{KY1} \cdot F'_{z0} \cdot \sin\Bigg(2 \cdot \operatorname{atan}(\frac{F_z}{P_{KY2} \cdot F'_{z0}})\Bigg) \cdot \lambda_{Ky\alpha} \tag{A.1g}$$

$$K_{y\alpha} = K_{y\alpha 0} \cdot (1 - P_{KY3} \cdot \gamma^{*2}) \cdot \xi_3 \tag{A.1h}$$

$$B_y = \frac{K_{y\alpha}}{C_y \cdot D_y} \tag{A.1i}$$

$$S_{Hy} = (P_{HY1} + P_{HY2} \cdot df_z) \cdot \lambda_{Hy} + P_{HY3} \cdot \gamma^* \cdot \lambda_{Ky\gamma} \cdot \xi_0 + \xi_4 - 1 \tag{A.1j}$$

$$S_{Vy} = F_z \cdot \Big((P_{VY1} + P_{VY2} \cdot df_z) \cdot \lambda_{Vy} + (P_{VY3} + P_{VY4} \cdot df_z) \cdot \gamma^* \cdot \lambda_{Ky\gamma}\Big) \lambda'_{\mu y} \cdot \xi_2 \tag{A.1k}$$

Similar as for the lateral force the aligning torque for pure side slip can be extended to following:

$$M_{z0} = M'_{z0} + M_{zr0} \tag{A.2a}$$

$$M'_{z0} = -t_0 \cdot F_{y0} \tag{A.2b}$$

$$t_0 = t(\alpha_t) = D_t \cdot \cos\Bigg(C_t \cdot \operatorname{atan}\Big(B_t \cdot \alpha_t - E_t \cdot (B_t \cdot \alpha_t - \operatorname{atan}(B_t \cdot \alpha_t))\Big)\Bigg) \cdot \cos'(\alpha) \tag{A.2c}$$

$$\alpha_t = \alpha^* + S_{Ht} \tag{A.2d}$$

$$S_{Ht} = Q_{HZ1} + Q_{HZ2} \cdot df_z + (Q_{HZ3} + Q_{HZ4} \cdot \gamma^*) \tag{A.2e}$$

$$M_{zr0} = M_{zr}(\alpha_r) = D_r \cdot \cos\Big(C_r \cdot \operatorname{atan}(B_r \cdot \alpha_r)\Big) \tag{A.2f}$$

$$\alpha_r = \alpha^* + S_{Hf} \tag{A.2g}$$

$$K'_{y\alpha} = K_{y\alpha} + \epsilon_K \tag{A.2h}$$

$$B_t = (Q_{BZ1} + Q_{BZ2} \cdot df_z + Q_{BZ3} \cdot df_z^2) \cdot (1 + Q_{BZ5}|\gamma^*| + Q_{BZ6} \cdot \gamma^{*2}) \cdot \frac{\lambda_{Ky\alpha}}{\lambda_{\mu y}}^* \quad (> 0) \tag{A.2i}$$

$$C_t = Q_{CZ1} \quad (> 0) \tag{A.2j}$$

$$D_{t0} = F_z \cdot (\frac{R_0}{F'_{z0}}) \cdot (Q_{DZ1} + Q_{DZ2} \cdot df_z) \cdot \lambda_t \cdot \operatorname{sign}(V_{cx}) \tag{A.2k}$$

$$D_t = D_{t0} \cdot (1 + Q_{DZ3} \cdot |\gamma^*| + Q_{DZ4} \cdot \gamma^{*2}) \cdot \xi_5 \tag{A.2l}$$

$$E_t = (Q_{EZ1} + Q_{EZ2} \cdot df_z + Q_{EZ3} \cdot df_z^2) \cdot \Big(1 + (Q_{EZ4} + Q_{EZ5} \cdot \gamma^*) \cdot \frac{2}{\pi} \cdot \operatorname{atan}(B_t \cdot C_t \cdot \alpha_t)\Big) \quad (\leq 1) \tag{A.2m}$$

$$B_r = (Q_{EZ9} \cdot \frac{\lambda_{Ky}}{\lambda^*_{\mu y}} + Q_{BZ10} \cdot B_y \cdot C_y) \cdot \xi_6 \tag{A.2n}$$

$$C_r = \xi_7 \tag{A.2o}$$

$$\begin{aligned} D_r = & F_z \cdot R_0 \cdot \Big((Q_{DZ6} + Q_{DZ7} \cdot df_z) \cdot \lambda_{Mr} \cdot \xi_2 + (Q_{DZ8} + Q_{DZ9} \cdot df_z) \cdot \gamma^* \cdot \lambda_{Kz\gamma} \cdot \xi_0\Big) \\ & \cdot \cos'(\alpha) \cdot \lambda^*_{\mu y} \cdot \operatorname{sign}(V_{cx}) + \xi_8 - 1 \end{aligned} \tag{A.2p}$$

$$K_{z\gamma 0} = D_{t0} \cdot K_{y\alpha 0} \tag{A.2q}$$

$$K_{z\gamma 0} = F_z \cdot R_0 \cdot (Q_{DZ8} + Q_{DZ9} \cdot df_z) \cdot \lambda_{Kz\gamma} - D_{t0} \cdot K_{y\gamma 0} \tag{A.2r}$$

B Vehicle Model Creation

K&C data from the SPMM-rig together with damper data from the damper rig was used to build the vehicle model in CRT. All measurement data needed to build the vehicle model from the K&C-rig were given in a folder in .txt-format. These files were renamed to the names used in the K&C-configuration file in CRT. The K&C-configuration file is a list that sort out the right measurement data with the corresponding function in car real time. If using more than one vertical state, bounce level, the maximum and minimum is defined here with an specific suffix such as "*_up*" "*_dn*" in the end of the data file name. One starts with creating a new database in CRT. This is were the new model will be saved. To create the model the vehicle model wizard tool was used. Here one defines the location of the wanted K&C-configuration file and selects the directory of one of the corresponding metrics data files. Next step is to define specific tyres used and import damper data. The damping data was measured in the damper rig at Volvo Torslanda and was retrieved in a late state of the project. The damper compression ratio versus wheel vertical displacement was not measured and had to be taken from other K&C-data from earlier measurement performed outside this project. The steering kinematics when using steering wheel angle input was automatically imported when using the vehicle wizard. In order to achieve information about rack displacement and rack forces one had to convert the steering kinematic table to the correct rack properties, see figure B. This was done by exporting the tables valid for steering wheel angles into rack travel. The first column in these tables were then converted from steering wheel angle to the corresponding rack displacement. The ratio between steering wheel angle and rack travel was calculated separately by using the data from the SPMM-rig.

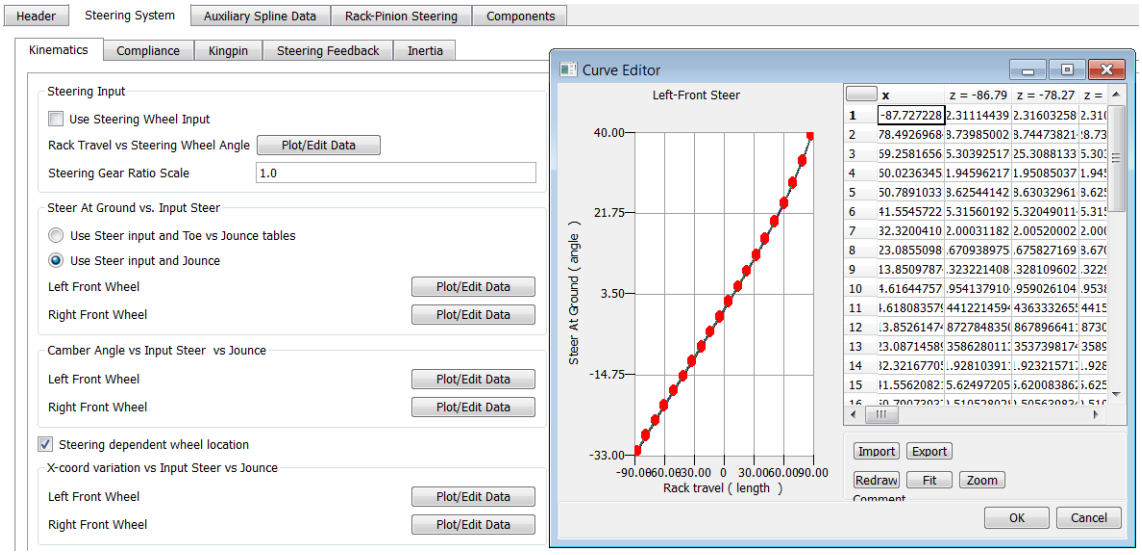

Figure B.1: Steering wheel angle to rack displacement ratio inserted into CRT

The steering geometry presented in figure B data was defined in the K&C-measurement report and put into the model. The x-values was set as the measured caster trail for that wheel. The y-values was set to the according to SPMM-calculation manual [3] as the kingpin offset. The z-values was set as the vertical height of the hub but with a minus sign to match the used defined coordinate system.

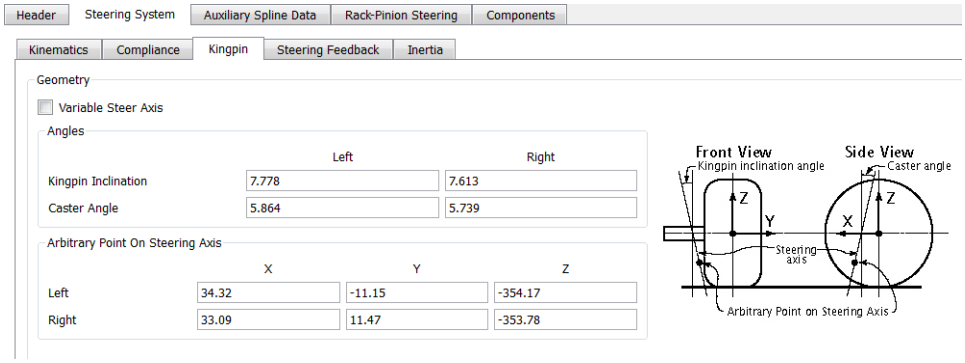

Figure B.2: Steering geometry inserted into CRT

C Steering model topology

Topology over the derived steering system used in this thesis. Green is the base torque table. Red is the friction algorithm and purple is the damping algorithm.

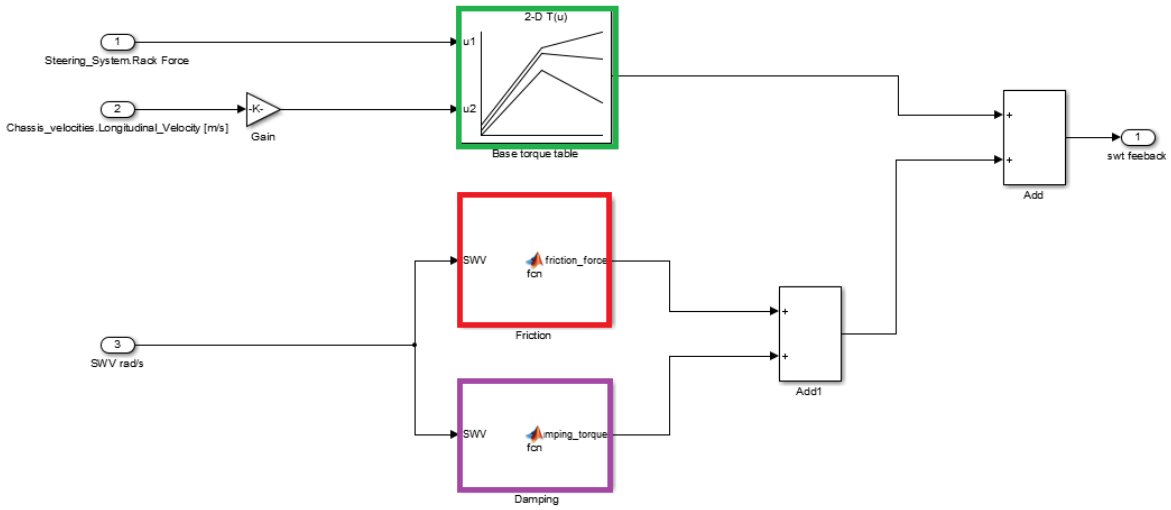

Figure C.1: Steering system topology containing base torque, friction and damping